J. Fluid Mech. (2008), *vol.* 595, *pp.* 45–82.
doi:10.1017/S0022112007008750 Printed in the United Kingdom

Stability of detonations for an idealized condensed-phase model

M. SHORT[1]†, I. I. ANGUELOVA[2], T. D. ASLAM[3], J. B. BDZIL[3], A. K. HENRICK[3,4] AND G. J. SHARPE[3]‡

[1]Theoretical and Applied Mechanics, University of Illinois, Urbana, IL 61801, USA
[2]Department of Mathematics, University of Illinois, Urbana, IL 61801, USA
[3]Los Alamos National Laboratory, Los Alamos, NM 87545, USA
[4]Department of Aerospace and Mechanical Engineering, University of Notre Dame, Notre Dame, IN 46556, USA

(Received 21 January 2005 and in revised form 3 August 2007)

The stability of travelling wave Chapman–Jouguet and moderately overdriven detonations of Zeldovich–von Neumann–Döring type is formulated for a general system that incorporates the idealized gas and condensed-phase (liquid or solid) detonation models. The general model consists of a two-component mixture with a one-step irreversible reaction between reactant and product. The reaction rate has both temperature and pressure sensitivities and has a variable reaction order. The idealized condensed-phase model assumes a pressure-sensitive reaction rate, a constant-γ caloric equation of state for an ideal fluid, with the isentropic derivative $\gamma = 3$, and invokes the strong shock limit. A linear stability analysis of the steady, planar, ZND detonation wave for the general model is conducted using a normal-mode approach. An asymptotic analysis of the eigenmode structure at the end of the reaction zone is conducted, and spatial boundedness (closure) conditions formally derived, whose precise form depends on the magnitude of the detonation overdrive and reaction order. A scaling analysis of the transonic flow region for Chapman–Jouguet detonations is also studied to illustrate the validity of the linearization for Chapman–Jouguet detonations. Neutral stability boundaries are calculated for the idealized condensed-phase model for one- and two-dimensional perturbations. Comparisons of the growth rates and frequencies predicted by the normal-mode analysis for an unstable detonation are made with a numerical solution of the reactive Euler equations. The numerical calculations are conducted using a new, high-order algorithm that employs a shock-fitting strategy, an approach that has significant advantages over standard shock-capturing methods for calculating unstable detonations. For the idealized condensed-phase model, nonlinear numerical solutions are also obtained to study the long-time behaviour of one- and two-dimensional unstable Chapman–Jouguet ZND waves.

1. Introduction

A detonation is a form of propagating wavefront that can occur in gaseous, liquid or solid explosives. It has a structure consisting of a lead shock which is sustained

† Present address: Los Alamos National Laboratory, Los Alamos, NM 87545, USA.
‡ Present address: School of Mechanical Engineering, University of Leeds, Leeds LS2 9JT, UK.

by chemical reaction in a following reaction zone. In gases, detonation fronts tend to propagate in a highly unsteady manner, the most common illustration of which is the formation of spectacular fish-scale patterns on the walls of rectangular shock tubes lined with soot-covered aluminium foil (Fickett & Davis 1979). Detonation speeds in gases occur in the range of 1000–2000 m s^{-1}, with peak shock pressures of the order of 10–100 kPa. On the other hand, in solid explosives, detonation speeds occur in the range 6000–8000 m s^{-1}, with peak pressures of the order of tens of gigapascals (Fickett & Davis 1979).

The mathematical and numerical modelling of detonation waves is almost invariably undertaken in the context of the compressible, inviscid Euler equations of motion accounting for heat addition from chemical reaction. Steady, planar detonation wave solutions can be constructed in the context of this model. The most familiar are known as ZND waves, after Zeldovich, von Neumann and Döring (Fickett & Davis 1979). The ZND wave profile consists of a sharp (discontinuous) shock front, followed by a finite zone of chemical reaction (in which the flow is subsonic relative to the shock), which terminates at a location termed here as the 'final point'. The (inert) flow downstream of the final point is dependent on the nature of the rear boundary. Fickett & Davis (1979) restrict the term ZND to the case of a single irreversible reaction of positive thermicity (a quantity which measures the conversion of chemical bond energy to macroscopic translational energy), and we will adopt this convention in the following. Each wave of ZND type has a minimum sustainable detonation speed, D_{CJ}, known as the Chapman–Jouguet (or CJ) speed where a sonic flow point (relative to the detonation shock) arises at the final point. Such waves have the property that the reaction zone between the shock and sonic point is acoustically isolated from the flow structure downstream of the sonic point. Any ZND wave travelling with a speed higher than D_{CJ} is called overdriven, and must be mechanically supported in some fashion, e.g. by a driving piston. In this case, the region of flow between the shock and supporting boundary is subsonic. Between the final point and the supporting boundary there is a region of spatially uniform flow. For waves of CJ type, the detonation can be supported, in which case the region downstream of the final point consists of sonic spatially uniform flow, or unsupported, in which case there is a region of unsteady supersonic flow downstream of the sonic final point, where an expansion (or Taylor) wave connects the state at the final point to the rear boundary. In some cases, the Taylor wave may not be directly attached to the final point.

In gaseous explosives, such steady, planar solutions are rarely observed in practice. Consequently, the linear and nonlinear stability of steady, planar, gas phase detonations has been studied extensively via analytical and numerical investigations. These analyses are based on a flow model consisting of the reactive form of the Euler equations, as discussed above, but in addition assume caloric and thermal equations of state for an ideal reactive gas. The most commonly studied reaction model involves an assumption of one-step, irreversible, mole-preserving chemistry with an Arrhenius temperature-sensitive rate form and simple depletion (i.e. unit reaction order). With these assumptions, we will label this system as the idealized gas phase model. Analyses of the linear stability properties of detonations governed by the idealized gas phase model, that solve the linearized system without asymptotic approximation, include those by Erpenbeck (1964), Lee & Stewart (1990), Bourlioux, Majda & Roytburd (1991*a*), Bourlioux & Majda (1992), Sharpe (1997) and Short & Stewart (1998). All these studies, except Erpenbeck (1964), employ a normal-mode approach. These papers highlight a bifurcation parameter family consisting of four

primary members: the detonation overdrive, the activation energy of the reaction, the heat release and the isentropic derivative. Although there are exceptions, the basic stability behaviour within certain ranges can be characterized as follows: detonations tend to become unstable to one- and multi-dimensional disturbances for decreasing overdrive, increasing heat release, increasing activation energy and decreasing isentropic derivative. Several linear stability studies of detonations with more complex reaction models have also been conducted, including two-step models (e.g. Short & Sharpe 2003), three-step (e.g. Short & Dold 1996; Short & Quirk 1997; Sanchez *et al.* 2001) and pathological models (e.g. Sharpe 1999). Gorchkov *et al.* (2007) have recently presented a stability formulation that applies to general equations of state and arbitrarily complex reaction mechanisms.

Most of the studies on nonlinear detonation stability have been conducted via high resolution numerical simulation of detonations governed by the idealized gas phase model (e.g. Bourlioux *et al.* 1991*a*; Bourlioux & Majda 1992; Sharpe & Falle 1999; Gamezo *et al.* 2000; Sharpe 2001; Ng *et al.* 2005; Henrick, Aslam & Powers 2006; Henrick 2007). These studies appear to capture successfully the main form of (quasi) one-dimensional instabilities observed experimentally, including single-period limit cycle oscillations, period-doubling bifurcated solutions and apparently chaotic evolutions. They also capture the multi-dimensional fish-scale patterns caused by the propagation of triple shock point interactions transverse to the main detonation front. These basic features remain when multi-step chemistry is employed (e.g. Radulescu *et al.* 2002). In addition to the direct simulation approaches, both one- and two-dimensional weakly nonlinear evolution equations about linear neutral stability points have also been constructed (Bourlioux *et al.* 1991*a*; Majda & Roytburd 1992). Several asymptotic approaches also have been formulated for investigating the linear and nonlinear stability of detonation, that invoke a limiting decomposition of the underlying steady wave to make analytical progress. Examples include include low-frequency formulations (e.g. Yao & Stewart 1996; Short & Sharpe 2003), high overdrive limits (e.g. Clavin & He 1996; Clavin, He & Williams 1997) and weak heat release limits (e.g. Short & Stewart 1999; Clavin & Williams 2002; Daou & Clavin 2003).

On the other hand, quantification of the reaction wave structure in detonating liquid and solid explosives is limited. The extreme high-pressure environment ($\sim$30–50 GPa), high wave speeds (6–8 km s^{-1}) and the lack of optical transparency of solid explosives make experimental diagnostic data collection and imaging difficult. Moreover, unlike in gases, the high pressure of the product materials in detonating condensed-phase explosives means there is no concept of a rigid confining wall. Particularly for lightly confined explosives, the wall compressibility (low impedance) and lateral expansion of the flow at the charge edge would act as a poor reflector of any transverse waves generated by an unstable detonation front. In addition, for light confinement, so-called failure waves can be generated at the confiner boundary. These interact with each other in a similar fashion to triple point interactions in gas phase detonations, forming patterns similar to those observed on soot foil records, but their structure is different from the triple shock wave structure seen in gaseous detonations (Fickett & Davis 1979).

That said, there is convincing experimental evidence that detonations in acetone-diluted and heterogeneous liquid nitromethane do exhibit an irregular unstable front structure (Davis 1981; Engelke & Bdzil 1983). On the other hand, laser-based interferometry measurements of particle velocities in the reaction zone of several other condensed-phase explosives do not indicate any evidence of large-scale spatial instabilities. Such measurements have been conducted for detonations in pure and commercial grade liquid nitromethane (Sheffield *et al.* 2002), in the heterogeneous

HMX-based solid explosive PBX-9501 (Gustavsen, Sheffield & Alcon 2000), and in the TATB-based solid explosive PBX-9502 (Seitz *et al.* 1989). Since the particle velocity traces are broadly reproducible for a given explosive, one can conclude that the underlying reaction zone structure must be close to the idealized one-dimensional ZND structure, and that any three-dimensional multi-wave instability that is present would have to be of significantly smaller amplitude than the bulk one-dimensional spatial variation through the reaction zone (Sheffield *et al.* 2002). Measurements of velocity against front curvature for detonations propagating in cylindrical sticks of PBX-9502 (Hill, Bdzil & Aslam 2002) show a very regular continuous variation, a finding that also reinforces this conclusion. Based on these observations, it would appear that detonations in a majority of condensed-phase explosives (except for certain forms of diluted nitromethane) do not show significant time-dependent reaction zone instability.

From a modelling viewpoint, the ability to accurately predict detonation behaviour in condensed-phase explosives is hampered by the lack (and complexity) of accurate equations of state and of suitable reaction models. One popular, and straightforward, model that is often used in the context of condensed-phase detonation modelling consists of a one-step, irreversible reaction with a pressure-sensitive reaction rate (r) of the form

$$r = k(1-\lambda)^{\nu} p^{n}, \tag{1.1}$$

where k is a rate constant, λ is a reaction progress variable, ν is the reaction order, and n is a measure of the pressure sensitivity. Upstream pressure is ignored (the so-called strong shock limit). This model also consists of a constant-γ caloric equation of state appropriate to an ideal gas, in which the isentropic derivative γ is assumed to take the value $\gamma = 3$. The choice of γ gives a detonation pressure at the CJ point that is in the appropriate range for condensed-phase systems. This model, which we hereafter now refer to as the 'idealized condensed-phase model', has been extensively used for the theoretical analysis of the properties of condensed-phase detonations (Fickett & Davis 1979; Bdzil *et al.* 2003). Pressure-sensitive reaction rates are also one of the primary components of the popular 'ignition and growth' style of reactive burn models commonly used for modelling detonations in high explosive systems (Lee & Tarver 1980; Tarver, Kury & Breithaupf 1997).

The main concern of the present paper is the study of the stability of steady, planar (ZND) detonations for the idealized condensed-phase model. The ZND detonation structure defined by this model has some interesting properties that distinguishes itself from the ZND detonation structure obtained from the idealized gas phase model. For instance, the reaction rate always takes its maximum at the shock. Also, while for simple depletion ($\nu = 1$) the reaction zone is formally of infinite spatial extent for both overdriven ($f > 1$) and Chapman–Jouguet ($f = 1$) waves (as it is for $\nu > 1$), for sub-unity reaction orders, $\nu < 1$, the reaction zone is of finite spatial extent for $f \geqslant 1$. Here f represents the detonation overdrive factor. In addition, for overdriven waves with $\nu > 0$, the thermodynamic state variables all possess a zero spatial gradient at the final point (where $\lambda = 1$), as is the case for Chapman–Jouguet ($f = 1$) waves with $\nu > 1/2$. For square-root depletion ($\nu = 1/2$) and $f = 1$, the thermodynamic variables have a finite spatial gradient at $\lambda = 1$, and for $f = 1$, $\nu < 1/2$, this spatial gradient is infinite at $\lambda = 1$. In this paper, we restrict the reaction order to lie in the range $1/2 \leqslant \nu \leqslant 1$. For the linear stability analysis, we will consider both CJ ($f = 1$) and moderately overdriven waves ($f > 1$, $f - 1 = O(1)$). The analysis for weakly overdriven waves, $f - 1 \ll 1$, will be considered in a future article.

The paper is laid out as follows: in § 2, we provide a description of the general detonation model, from which both the idealized condensed-phase and gas-phase models can be extracted. The ZND detonation structure for the idealized condensed-phase model for both CJ and moderately overdriven waves is explored in § 3. In § 4, the linear stability analysis of a ZND detonation for the general detonation model is formulated using a normal-mode approach. Of particular importance for this analysis is the derivation of appropriate spatial boundedness conditions at the end of the steady reaction zone for the eigenfunction system. This is studied in § 5, where it is found that closure conditions are required that cover six different cases: for CJ waves ($f=1$) with reaction orders $\nu=1/2$, $1/2<\nu<1$, and $\nu=1$; and for moderately overdriven waves ($f>1$, $f-1=O(1)$) with reaction orders $\nu=1/2$, $1/2<\nu<1$ and $\nu=1$. In § 6, additional comments are made regarding the role of the transonic layer at the end of the detonation reaction zone for CJ detonations in the linear stability formulation, and on the nature of the decay of linearly perturbed stable detonations. In § 7, solutions of the linear stability formulation for ZND detonation waves defined by the idealized condensed-phase model are presented. Comparisons of the predictions of the normal-mode analysis with some one- and two-dimensional direct numerical integration calculations of unstable detonation waves under the idealized condensed-phase model are made in § 8. In § 9, one- and two-dimensional nonlinear evolutions of unstable Chapman–Jouguet detonations for the idealized condensed-phase model are investigated.

2. General detonation model

2.1. *Equations*

The non-dimensional equations of motion coupled with an equation for species conservation for the two component reaction $\mathscr{F}\rightarrow\mathscr{P}$ are given by

$$\frac{\mathrm{D}v}{\mathrm{D}t^l}-v(\nabla^l\cdot\boldsymbol{u}^l)=0,\quad \frac{\mathrm{D}\boldsymbol{u}^l}{\mathrm{D}t^l}=-v\nabla^l p,\quad \frac{\mathrm{D}e}{\mathrm{D}t^l}=-pv(\nabla^l\cdot\boldsymbol{u}^l),\quad \frac{\mathrm{D}\lambda}{\mathrm{D}t^l}=\bar{W}(p,v,\lambda),\tag{2.1}$$

for the volume v, pressure p, specific internal energy e, laboratory frame velocity $\boldsymbol{u}^l=(u^l,w^l)$ and reaction progress variable λ ($=1-$fuel mass fraction). We adopt the constant-γ caloric equation of state appropriate for an ideal gas,

$$e=e(p,v,\lambda)=\frac{pv}{(\gamma-1)}-Q\lambda,\tag{2.2}$$

where Q is the heat of reaction in converting $\mathscr{F}$ to $\mathscr{P}$, and γ is the isentropic derivative. The (chemically) frozen sound speed c is obtained from (2.2) as

$$c^2=v^2(p+e_{,v})/e_{,p}=\gamma pv.\tag{2.3}$$

The reaction rate is given by

$$\bar{W}=\begin{cases}kp^n(1-\lambda)^\nu\exp(-\theta/pv), & 0\leqslant\lambda<1,\\ 0, & \lambda=1,\end{cases}\tag{2.4}$$

where $\lambda=0$ represents unreacted fuel and $\lambda=1$ is fully depleted fuel. This rate choice has three variable components: an algebraic pressure sensitivity measured by n, an Arrhenius temperature sensitivity measured by the activation energy θ, and the reaction (or depletion) order ν. The one-step reaction model with a fractional or integer reaction order represents a global approximation to a complex

set of reactions that occur during the detonation of high explosives, and is an approximation frequently employed in detonation modelling studies (Fickett & Davis 1979; Bdzil *et al.* 2003). For this study, the reaction order is taken to lie in the range $1/2 \leqslant \nu \leqslant 1$.

The above equations have been non-dimensionalized such that

$$\left.\begin{gathered} v = \frac{\tilde{v}}{\tilde{v}_u}, \quad \boldsymbol{u} = \frac{\tilde{\boldsymbol{u}}}{\widetilde{D}}, \quad p = \frac{\tilde{p}}{\widetilde{D}^2/\tilde{v}_u}, \quad \boldsymbol{x} = \frac{\tilde{\boldsymbol{x}}}{\tilde{l}}, \quad t = \frac{\tilde{t}}{\tilde{l}/\widetilde{D}}, \\ e = \frac{\tilde{e}}{\widetilde{D}^2}, \quad c^2 = \frac{\tilde{c}^2}{\widetilde{D}^2}, \quad Q = \frac{\widetilde{Q}}{\widetilde{D}^2}, \quad \theta = \frac{\widetilde{E}}{\widetilde{D}^2}, \end{gathered}\right\} \tag{2.5}$$

where $\widetilde{v}_u$ is the upstream specific volume, $\widetilde{D}$ is the dimensional (ZND) planar steady detonation velocity and $\widetilde{E}$ is the dimensional activation energy. The rate constant k is determined by the reference length scale $\tilde{l}$ which sets $\lambda = 1/2$ at $x = 1$ in the non-dimensionalized ZND wave, i.e. the standard half-reaction length scaling.

For ease of analysis, we now introduce a reaction progress variable transformation given by

$$\beta = (1 - \lambda)^{1/2}, \tag{2.6}$$

where $\beta = 1$ is unreacted fuel and $\beta = 0$ is fully depleted, whereupon the species conservation equation becomes

$$\frac{\mathrm{D}\beta}{\mathrm{D}t} = -\frac{1}{2} k p^n \beta^{2\nu - 1} \exp(-\theta/pv) = W. \tag{2.7}$$

Note that

$$W_{,p} = \left(\frac{n}{p} + \frac{\theta}{vp^2}\right) W, \quad W_{,v} = \frac{\theta}{v^2 p} W, \quad W_{,\beta} = (2\nu - 1)\frac{W}{\beta}, \tag{2.8}$$

so that $W_{,\beta} = 0$ for square-root depletion order ($\nu = 1/2$).

2.2. *Shock relations*

The equations of motion are subject to the standard set of Euler conservation laws across the lead shock front. Given a shock with velocity $\boldsymbol{V}^l = \boldsymbol{V}^l(\boldsymbol{x}^l, t)$, these jump relations are

$$\left.\begin{gathered} [\rho(\boldsymbol{u}^l - \boldsymbol{V}^l) \cdot \boldsymbol{n}^l] = 0, \quad [\rho \boldsymbol{u}^l (\boldsymbol{u}^l - \boldsymbol{V}^l) \cdot \boldsymbol{n}^l + p \boldsymbol{n}^l] = 0, \\ \left[m\left(e + \tfrac{1}{2}\boldsymbol{u}^l \cdot \boldsymbol{u}^l\right) + p(\boldsymbol{u}^l \cdot \boldsymbol{n}^l)\right] = 0, \end{gathered}\right\} \tag{2.9}$$

for shock normal $\boldsymbol{n}^l$, where

$$m = \rho(\boldsymbol{u}^l - \boldsymbol{V}^l) \cdot \boldsymbol{n}^l \tag{2.10}$$

is the constant mass flux across the shock, and the density $\rho = v^{-1}$. If the shock surface is $F(\boldsymbol{x}^l, t) = 0$, the shock normal and normal shock velocity are denoted by

$$\boldsymbol{n}^l = \frac{\nabla^l F}{|\nabla^l F|}, \quad \boldsymbol{V}^l \cdot \boldsymbol{n}^l = -\frac{1}{|\nabla^l F|} \frac{\partial F}{\partial t}. \tag{2.11}$$

2.3. *Idealized gas and condensed-phase models*

To define the idealized gas and condensed-phase detonation models, we introduce the parameter

$$\delta = \frac{\tilde{c}_u^2}{\tilde{D}_{CJ}^2}, \quad 0 \leqslant \delta < 1, \tag{2.12}$$

which represents the inverse of the square of the Chapman–Jouguet detonation Mach number ($\tilde{D}_{CJ}/\tilde{c}_u$). The idealized condensed-phase model is set by assuming an activation energy independent reaction rate ($\theta = 0$), the strong shock limit (defined by $\delta = 0$), and an isentropic derivative $\gamma = 3$. The ideal gas phase model is defined by assuming a pressure-independent reaction rate ($n = 0$), finite shock strength ($\delta > 0$), an isentropic derivative typically in the range $1 < \gamma \leqslant 1.6$, and simple reactant depletion ($\nu = 1$).

3. One-dimensional steady-state solutions

The above model supports a one-dimensional, steady, travelling wave solution. In a reference frame $x = x^l - t^l$, with a shifted velocity defined as $u = u^l - 1$, the travelling wave structure can be described in terms of the reaction variable β through the relations

$$\left.\begin{aligned} v &= -u, \quad p = 1 + \frac{\delta}{\gamma f} + u, \\ u &= -\frac{\gamma}{(\gamma+1)}\left(1 + \frac{\delta}{\gamma f}\right) + \frac{(1-\delta)}{(\gamma+1)\sqrt{f}}\left[(f-1)\frac{(1-\delta^2/f)}{(1-\delta)^2} + \beta^2\right]^{1/2}. \end{aligned}\right\} \tag{3.1}$$

Here f is the usual detonation overdrive factor, $f = D^2\delta$, where D is the detonation Mach number. The planar Chapman–Jouguet wave has $f = 1$, and is the limiting steady travelling wave in which the flow is identically sonic at the point of complete reaction (final point), or $c = -u$ at $\beta = 0$. The scaled heat of reaction Q is related to δ by

$$Q = \frac{(1-\delta)^2}{2f(\gamma^2 - 1)}, \tag{3.2}$$

so that in the strong shock limit ($\delta = 0$), $Q = 1/[2f(\gamma^2 - 1)]$. The detonation shock lies at $x = 0$, while the reaction zone structure lies in the region $x < 0$.

The spatial extent of the steady reaction zone for a given β is

$$x = \int_1^\beta \frac{u}{W}\,\mathrm{d}\beta \tag{3.3}$$

where for $f \geqslant 1$ as $\beta \to 0$, $W = O(\beta^{2\nu-1})$ and $u = O(1)$. Thus, for simple depletion ($\nu = 1$), $x = O(\ln\beta)$ as $\beta \to 0$, and so that the reaction zone formally has an infinite spatial extent for both Chapman–Jouguet ($f = 1$) and overdriven ($f > 1$) waves. On the other hand, for $1/2 \leqslant \nu < 1$, the integral (3.3) has the asymptotic behaviour $x = x_0 + O(\beta^{2(1-\nu)})$ as $\beta \to 0$, for a finite constant x_0, so that the reaction zone is of finite spatial extent for both Chapman–Jouguet and overdriven waves ($f \geqslant 1$). Also, the size of the spatial gradient of u (and consequently p and v from (3.1)) as $\beta \to 0$ is given by $u_{,x} = O(\beta^{2\nu})$ for moderately overdriven waves ($f > 1$, $f - 1 = O(1)$) and $u_{,x} = O(\beta^{2\nu-1})$ for $f = 1$. For depletion orders in the range $1/2 \leqslant \nu \leqslant 1$, the spatial gradients of the variables p, u and v in the steady travelling wave vanish at $\beta = 0$ for

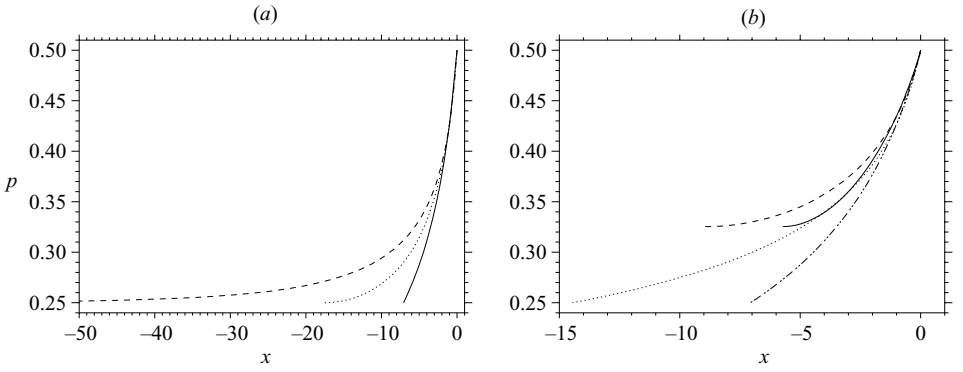

FIGURE 1. Steady wave pressure variation (p) with x for: (a) $f=1$, $n=2$, $\gamma=3$ and $\nu=1/2$ (solid), $\nu=3/4$ (dotted) and $\nu=1$ (dashed); (b) $\gamma=3$, $\nu=1/2$, and $n=2$, $f=1$ (dash-dot-dot-dot), $n=4$, $f=1$ (dotted), $n=2$, $f=1.1$ (solid), $n=4$, $f=1.1$ (dashed).

all overdriven waves, as they do for Chapman–Jouguet waves provided the depletion order is in the range $1/2<\nu\leqslant 1$. However, for $\nu=1/2$, $u_{,x}=O(1)$ as $\beta\to 0$, i.e. the spatial gradients of p, u and v are finite. Consequently, for supported Chapman–Jouguet waves there will be a discontinuity in $u_{,x}$ at $\beta=0$ for $\nu=1/2$, but $u_{,x}$ is continuous and equal to zero at $\beta=0$ for $1/2<\nu\leqslant 1$. Similarly, $u_{,x}$ is continuous and equal to zero for all overdriven waves with $1/2\leqslant\nu\leqslant 1$. Finally, the reaction rate $\bar{W}=0$ at $\lambda=1$ ($\beta=0$) for $1/2\leqslant\nu\leqslant 1$. However, for $\nu=1/2$, the rate of change of reaction rate, $\bar{W}_{,x}=O(1)$ at $\lambda=1$, while $\bar{W}_{,x}=0$ at $\lambda=1$ for $1/2<\nu\leqslant 1$. Thus, for $\nu=1/2$, the rate of change of reaction rate will be discontinuous at $\lambda=1$. In terms of the reaction coordinate β, these are equivalent to the conditions $W=O(1)$ for $\nu=1/2$ and $W=0$ for $1/2<\nu\leqslant 1$ at $\beta=0$.

We now examine some planar, steady detonation wave structures for the idealized condensed-phase model ($\theta=0, \delta=0$). Figure 1(a) shows the pressure variation through the steady Chapman–Jouguet ($f=1$) detonation reaction zone (up to the first point where $\beta=0$) for three reaction depletion orders, with $n=2$ and $\gamma=3$. Beyond the first equilibrium point (where $\beta=0$), there will be a uniform state corresponding to that shown at $\beta=0$ for supported Chapman–Jouguet waves, or typically a non-uniform, unsteady expansion wave state for unsupported waves. It is clearly seen that the detonation has a finite reaction zone length for $\nu<1$, which also increases in length as ν increases. Similarly, figure 1(b) shows that as n increases (for fixed $\nu(<1)$ and $f(\geqslant 1)$), the reaction zone increases in length, but also develops a significant reaction tail (e.g. for $f=1$, $\nu=1/2$, $\gamma=3$ and $n=8$, the steady reaction zone has a formal length of $x=-81.72$. However, one-half of the fuel ($0\leqslant\lambda\leqslant 1/2$) is depleted in the range $-1\leqslant x\leqslant 0$, while the remaining ($1/2\leqslant\lambda\leqslant 1$) is depleted over the much larger range $-81.72\leqslant x\leqslant -1$). For a fixed value of ν and n, the length of the reaction zone reduces in size as the wave becomes more overdriven, i.e. as f increases. Also, for square-root depletion ($\nu=1/2$) and Chapman–Jouguet waves ($f=1$), the spatial gradient of pressure ($p_{,x}$) is $O(1)$ at $\beta=0$, but for $\nu>1/2$, $p_{,x}=0$ at $\beta=0$ (figure 1a). For overdriven waves ($f>1$), on the other hand, $p_{,x}=0$ for $\nu\geqslant 1/2$ at $\beta=0$ (figure 1b).

Although the choice of $\gamma=3$ is an appropriate one for many liquid and solid explosives (Fickett & Davis 1979), it is instructive to examine the steady wave variation for other choices of γ ($\geqslant 2$). Figure 2 shows the pressure variation through

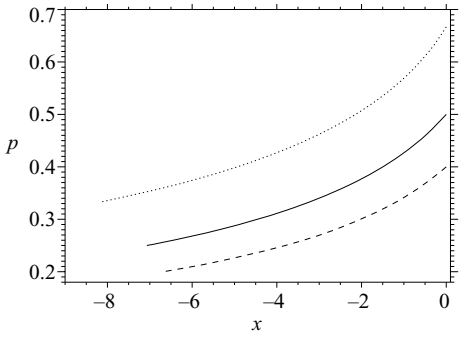

FIGURE 2. Steady wave pressure variation (p) with x for $f=1$, $n=2$, $\nu=1/2$ and $\gamma=2$ (dotted), $\gamma=3$ (solid), $\gamma=4$ (dashed).

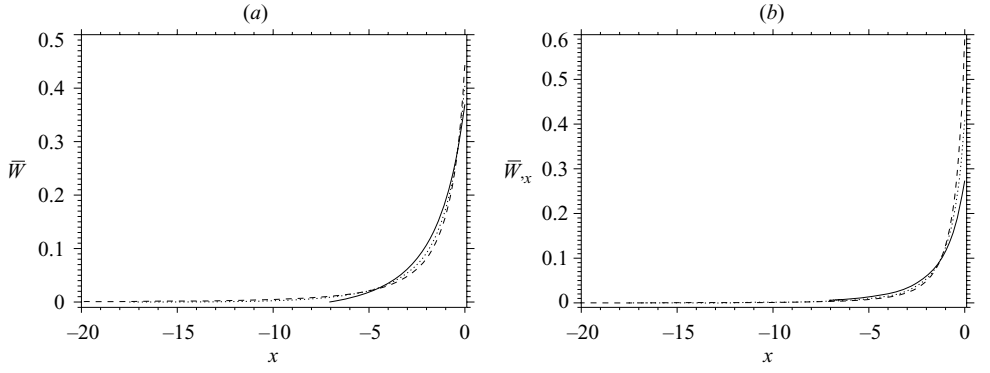

FIGURE 3. (*a*) Steady wave rate variation $\bar{W}$ and (*b*) steady wave rate of change of $\bar{W}$, $\bar{W}_{,x}$, with x for $n=2$, $\gamma=3$, $f=1$ with $\nu=1/2$ (solid), $\nu=3/4$ (dotted) and $\nu=1$ (dashed).

the steady detonation wave for $f=1$, $\nu=1/2$ and $n=2$ for various γ. For $\gamma=4$, the shock pressure is lower and the reaction zone length is shorter than that for $\gamma<4$. Decreasing γ increases the shock pressure, and lengthens the reaction zone. Finally, figure 3(*a*) shows the variation in the steady wave reaction rate $\bar{W}$ for $n=2$, $f=1$, $\gamma=3$ and $\nu=1/2$, $\nu=3/4$ and $\nu=1$. In all cases, since the pressure is a maximum at the shock, the reaction rate $\bar{W}$ is also a maximum there. This marks an important structural deviation from the standard temperature-sensitive Arrhenius rate law, where the reaction rate reaches a maximum at a point internal to the reaction zone, and typically closer to the final point than the shock. Figure 3(*b*) shows the corresponding rate gradient $\bar{W}_{,x}$, which is non-zero for $\nu=1/2$ at $\lambda=1$, but zero for $\nu>1/2$ at $\lambda=1$.

4. Linear stability analysis

Here the normal-mode linear stability analysis for the steady travelling wave detonation solutions identified in § 3 is outlined. Although this is carried out for the general detonation model, which incorporates both idealized gas and condensed-phase

systems, the stability results shown in § 7 will be specific to the idealized condensed-phase model.

4.1. *Coordinate transformation*

It is convenient to introduce a general coordinate transformation from (x^l, z^l, t^l) to (x, z, t) such that the shock location is fixed at $x = 0$, i.e.

$$x = x^l - t - \Psi(z, t), \quad z^l = z, \quad t^l = t, \tag{4.1}$$

where $x^l = t^l + \Psi(z^l, t^l)$ is the shock locus in the laboratory frame. Thus the gradient operator ∇ in the new frame is determined by the relations

$$\frac{\partial}{\partial x^l} = \frac{\partial}{\partial x}, \quad \frac{\partial}{\partial z^l} = -\frac{\partial \Psi}{\partial z}\frac{\partial}{\partial x} + \frac{\partial}{\partial z}, \quad \frac{\partial}{\partial t^l} = -\left(1 + \frac{\partial \Psi}{\partial t}\right)\frac{\partial}{\partial x} + \frac{\partial}{\partial t}. \tag{4.2}$$

We also define a new velocity vector $\boldsymbol{u}$, where $\boldsymbol{u}^l = \boldsymbol{u} + \boldsymbol{i}$.

4.2. *Stability equations*

The equations governing small (linear) perturbations to the steady travelling wave in § 3 are constructed via the linear expansion

$$\Psi = \epsilon \bar{\Psi}(z, t), \boldsymbol{z} = \boldsymbol{z}^* + \epsilon \bar{\boldsymbol{z}}(x, z, t), \epsilon \ll 1, \tag{4.3}$$

which corresponds to an $O(\epsilon)$ deviation from the ZND state, and where

$$\boldsymbol{z} = (v, u, w, p, \beta)^{\mathrm{T}} \tag{4.4}$$

represents the vector of dependent variables. The superscript * refers to the underlying steady wave solution. Normal-mode solutions to the $O(\epsilon)$ linearized system are then obtained via

$$\bar{\Psi} = \Psi_0 \mathrm{e}^{\alpha t + \mathrm{i}kz}, \quad \bar{\boldsymbol{z}} = \Psi_0 \boldsymbol{z}'(x)\mathrm{e}^{\alpha t + \mathrm{i}kz}, \quad \Psi_0 = O(1); \tag{4.5}$$

for growth rate α and wavenumber k, where the $'$ quantities indicate the (x) spatially dependent eigenfunctions.

For the present analysis, it will prove convenient to change the independent variable in the eigenfunctions from x to β^*, where $\beta^*_{,x} = W^*/u^*$, so that

$$\frac{\mathrm{d}}{\mathrm{d}x} = \frac{W^*}{u^*}\frac{\mathrm{d}}{\mathrm{d}\beta^*}. \tag{4.6}$$

After some algebra, we arrive at the set of equations that govern the linear stability of a detonation with the generalized rate (2.4), namely

$$\frac{W^*\eta^*}{u^*}\boldsymbol{z}'_{,\beta^*} = \widehat{\boldsymbol{A}}^*\boldsymbol{z}' + \hat{\boldsymbol{s}}^*, \tag{4.7}$$

where the matrix $\widehat{\boldsymbol{A}}^*$ is defined in terms of steady state quantities as

$$\widehat{\boldsymbol{A}} = -\begin{pmatrix} (\alpha\eta - Wuu_{,\beta})/u + 2\beta Q(\gamma-1)W_{,v} & (-\alpha u^2 + Wu_{,\beta}(c^2-3u^2)/u)/u \\ c^2 Wu_{,\beta}/u^2 - 2\beta Q(\gamma-1)W_{,v} & u(\alpha + 2Wu_{,\beta}/u) \\ 0 & 0 \\ -Wu_{,\beta}(u^2-2c^2)/u^2 - 2\beta Q(\gamma-1)W_{,v} & (\alpha c^2 + Wu_{,\beta}(c^2+u^2)/u)/u \\ -W_{,v}\eta/u & W\eta/u^2 \end{pmatrix}$$

$$\begin{pmatrix} \mathrm{i}ku^2 & -u(\alpha + \gamma Wu_{,\beta}/u) + 2\beta Q(\gamma-1)W_{,p} & 2Q(\gamma-1)(W+\beta W_{,\beta}) \\ -\mathrm{i}c^2 k & u(\alpha + \gamma Wu_{,\beta}/u) - 2\beta Q(\gamma-1)W_{,p} & -2Q(\gamma-1)(W+\beta W_{,\beta}) \\ \alpha\eta/u & -\mathrm{i}k\eta & 0 \\ -\mathrm{i}c^2 k & u(\alpha + \gamma Wu_{,\beta}/u) - 2\beta Q(\gamma-1)W_{,p} & -2Q(\gamma-1)(W+\beta W_{,\beta}) \\ 0 & -W_{,p}\eta/u & \alpha\eta/u - W_{,\beta}\eta/u \end{pmatrix} \tag{4.8}$$

and the vector $\boldsymbol{s}$ is

$$\begin{aligned} \boldsymbol{s} = -[&\alpha Wu_{,\beta}(3u^2-c^2)/u^2, -2W\alpha u_{,\beta}, \mathrm{i}kWu_{,\beta}\eta/u, \\ &-\alpha Wu_{,\beta}(c^2+u^2)/u^2, -\alpha W\eta/u^2]. \end{aligned} \tag{4.9}$$

The variable η is the sonic parameter for the steady wave defined as

$$\eta = u^2 - c^2. \tag{4.10}$$

4.3. *Shock relations*

Using the conservation relations (2.9) and expressions for the shock normal and velocity (2.11), the perturbation variables will satisfy the relations

$$\begin{gathered} u' = \frac{2(1+\delta/f)}{\gamma+1}\alpha, \quad p' = \frac{4}{\gamma+1}\alpha, \quad w' = -\frac{2(1-\delta/f)}{\gamma+1}\mathrm{i}k, \\ v' = -\frac{4\delta/f}{\gamma+1}\alpha, \quad \beta' = 0, \end{gathered} \tag{4.11}$$

at $\beta^* = 1$, assuming no reaction occurs in the shock.

5. Eigenfunction boundedness analysis

An additional boundary condition is required to close the system (4.7) through (4.11) in order to determine the eigenvalue α. Nominally, this must guarantee spatial boundedness of the eigenfunction system either at $\beta^* = 0$ or $x^* = -\infty$, as for the previously examined case of idealized gas phase detonations for simple depletion ($\nu = 1$) and for either Chapman–Jouguet ($f = 1$) or overdriven ($f > 1$) waves (Sharpe 1997). The spatial structure of the solutions to (4.7) as $\beta \to 0$ are obtained below.

From this point forward, we drop the superscript * that is used to denote steady wave components. Also, for the overdriven cases, we will only consider moderate overdrive where $f > 1$, $f - 1 = O(1)$. The structure for weakly overdriven systems where $f > 1$, $f - 1 \ll 1$, introduces some additional complications due to presence of both coordinate ($\beta \to 0$) and parameter expansions (in $f - 1$) that will be detailed in a separate paper. Consequently, the notation $f > 1$ used below is taken to imply the moderate overdrive limit $f > 1$, $f - 1 = O(1)$.

5.1. *Analysis of steady wave structure* $\beta \to 0$

Before evaluating the structure of the solutions of the system (4.7) in the limit $\beta \to 0$, some additional details on the structure of the steady travelling detonation in various regimes as $\beta \to 0$ are required.

First, some results for steady Chapman–Jouguet detonations ($f = 1$) and arbitrary depletion order ν are noted. The steady-state variation with β is obtained from (3.1), without approximation, as

$$u = u_0 + \beta u_1, \quad p = p_0 + \beta p_1, \quad v = v_0 + \beta v_1, \tag{5.1}$$

where

$$u_0 = -\frac{\gamma}{(\gamma+1)}\left(1 + \frac{\delta}{\gamma}\right), \quad p_0 = \frac{1}{(\gamma+1)}\left(1 + \frac{\delta}{\gamma}\right), \quad v_0 = -u_0. \tag{5.2}$$

Thus u, p and v are $O(1)$ as $\beta \to 0$, i.e. have finite amplitude at the end of the reaction zone. The sonic parameter ($\eta = u^2 - c^2$) in the steady wave is given by

$$\eta = \beta\tilde{\eta}, \quad \text{where} \quad \tilde{\eta} = \tilde{\eta}_0 + \beta\tilde{\eta}_1 \quad \text{and} \quad \tilde{\eta}_0 = -\frac{(1-\delta)(\gamma+\delta)}{\gamma+1}, \tag{5.3}$$

again without approximation, so that $\eta = O(\beta)$ as $\beta \to 0$, i.e. vanishes at the end of the reaction zone for Chapman–Jouguet waves. Also, the velocity gradient with respect to β is given by

$$u_{,\beta} = \frac{1-\delta}{\gamma+1} = u_1, \tag{5.4}$$

so that $u_{,\beta} = O(1)$ as $\beta \to 0$, i.e. has a finite amplitude for $f = 1$ at $\beta = 0$.

On the other hand, for overdriven detonations ($f > 1$), again with arbitrary depletion order ν, the steady-state variables are expanded in the form

$$u \sim u_0 + O(\beta^2), \quad p \sim p_0 + O(\beta^2), \quad v \sim v_0 + O(\beta^2) \tag{5.5}$$

as $\beta \to 0$, where

$$\left.\begin{aligned} u_0 &= -\frac{\gamma}{(\gamma+1)}\left(1 + \frac{\delta}{\gamma f}\right) + \frac{(f-1)(1-\delta^2/f)}{(\gamma+1)\sqrt{f}(1-\delta)}, \quad v_0 = -u_0, \\ p_0 &= \frac{1}{(\gamma+1)}\left(1 + \frac{\delta}{\gamma f}\right) + \frac{(f-1)(1-\delta^2/f)}{(\gamma+1)\sqrt{f}(1-\delta)}. \end{aligned}\right\} \tag{5.6}$$

In this case, the sonic parameter $\eta = O(1) < 1$ at $\beta = 0$, i.e. the flow is subsonic at the final point. The velocity gradient $u_{,\beta}$ is such that $u_{,\beta} = O(\beta)$ as $\beta \to 0$, i.e. vanishing for overdriven waves at $\beta = 0$. Figure 4*a* shows an example of the different limiting behaviours of the steady detonation velocity gradient near $\beta = 0$ for $f = 1$ and $f = 1.1$, under the idealized condensed-phase model ($\delta = 0$, $\theta = 0$, $\gamma = 3$).

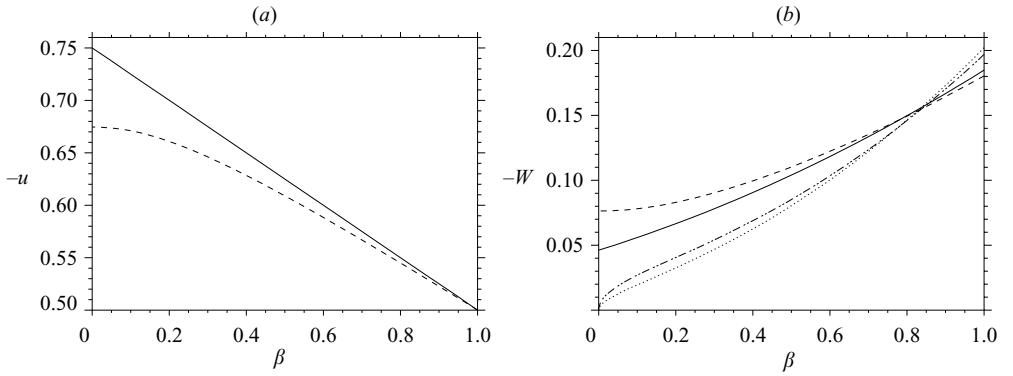

FIGURE 4. (*a*) Steady velocity variation with β for $n=2$, $\nu=1/2$ and $f=1$ (solid), $f=1.1$ (dashed). (*b*) Steady rate variation with β for $n=2$, and $f=1$, $\nu=1/2$ (solid), $f=1$, $\nu=0.75$ (dotted), $f=1.1$, $\nu=0.5$ (dashed) and $f=1.1$, $\nu=3/4$ (dash-dot-dot-dot).

Finally, for arbitrary ν, the reaction rate (W) has the asymptotic form

$$W=\widetilde{W}\beta^{2\nu-1}, \quad \text{where} \quad \widetilde{W}\sim\widetilde{W}_0+\beta\widetilde{W}_1+O(\beta^2) \quad \text{and} \quad \widetilde{W}_0=-\frac{kp_0^n}{2}\mathrm{e}^{-\theta/p_0v_0}. \tag{5.7}$$

For overdriven waves ($f>1$), the $O(\beta)$ correction to $\widetilde{W}$ vanishes, i.e. $\widetilde{W}_1=0$, but for Chapman–Jouguet waves ($f=1$), $\widetilde{W}_1=O(1)$. Also, for depletion orders in the range $1/2<\nu\leqslant 1$, $W\sim o(1)$ as $\beta\to 0$ with W vanishing at $\beta=0$, but for square-root depletion $\nu=1/2$, $W\sim O(1)$, i.e. has finite amplitude at $\beta=0$. The various behaviours for W are shown in figure 4(*b*).

With the results (5.1)–(5.7) in hand, an examination of the linear system (4.7)–(4.10) reveals that there are two potential sources of singular behaviour for the eigenfunction solutions as $\beta\to 0$. These are associated with the vanishing of steady sonic parameter, $\eta\to 0$, which occurs for Chapman–Jouguet waves, and/or a zero in the reaction rate $W\to 0$, which may occur for depletion orders $\nu>1/2$. In all, six different cases need to be considered, and these are examined in § 5.3–5.5 below. It is found that for $f=1$, $\beta=0$ is an irregular singular point for $1/2<\nu\leqslant 1$, and a regular singular point for $\nu=1/2$. For $f>1$, $f-1=O(1)$, $\beta=0$ is a regular singular point for $\nu=1$ and an ordinary point for $\nu<1$. For each case, asymptotic solutions to (4.7) for $\beta\to 0$ can be found in the form

$$z'=\sum_{i=1}^{5}C_i z'_{hi}+z'_p, \tag{5.8}$$

where the z'_{hi} and z'_p correspond to homogeneous and particular solutions respectively of (4.7) in the limit $\beta\to 0$, and the C_i are complex constants.

5.2. *Equilibrium zone analysis when $\beta=0$ is an ordinary point*

Before examining each specific case, we need to obtain some additional information about the spatial behaviour of perturbations in the equilibrium zone of a detonation when $f>1$ and $1/2\leqslant\nu<1$. As noted above, it transpires that $\beta=0$ is an ordinary point of the system (4.7) for cases in which both $1/2\leqslant\nu<1$ and $f>1$. An analysis beyond the point $\beta=0$ is then required to determine the appropriate boundedness condition. When $\nu<1$, the steady travelling detonation has a reaction zone of finite spatial extent (independently of whether $f=1$ or $f>1$), and for overdriven waves

($f > 1$) an equilibrium region of uniform, subsonic flow must exist beyond the end of the reaction zone. Unsteady linear perturbations to the uniform state in this region, of the normal-mode form (4.5), will satisfy the equations

$$z'_{a,x} = \widetilde{\boldsymbol{A}}_0 z'_a, \quad z_a = (v, u, w, p)^{\mathrm{T}} \tag{5.9}$$

where

$$\tilde{\boldsymbol{A}} = -\frac{1}{\eta}\begin{pmatrix} \alpha\eta/u & -\alpha u & \mathrm{i}ku^2 & -\alpha u \\ 0 & \alpha u & -\mathrm{i}c^2k & \alpha u \\ 0 & 0 & \alpha\eta/u & -\mathrm{i}k\eta \\ 0 & \alpha c^2/u & -\mathrm{i}c^2k & \alpha u \end{pmatrix}, \tag{5.10}$$

and the subscript zero is used to denote steady state conditions at $\beta = 0$. The eigenvalues of $\widetilde{\boldsymbol{A}}_0$ are

$$\lambda_1 = -\frac{\alpha}{\eta_0}(u_0 - c_0\omega), \quad \lambda_2 = -\frac{\alpha}{\eta_0}(u_0 + c_0\omega), \quad \lambda_{3,4} = -\frac{\alpha}{u_0}, \tag{5.11}$$

where

$$\omega = \sqrt{1 - \eta_0 k^2/\alpha^2}. \tag{5.12}$$

taking $\mathrm{Re}(\omega) > 0$. The solution for z'_a is

$$z'_a = \sum_{i=1}^{4} C_i \boldsymbol{r}_i \mathrm{e}^{\lambda_i x}, \tag{5.13}$$

where the C_i are complex constants, and the eigenvectors $\boldsymbol{r}_i$ are given by

$$\left.\begin{aligned} \boldsymbol{r}_1 &= [-\mathrm{i}u\alpha(c - u\omega)/c\eta k, \mathrm{i}\alpha(u - c\omega)/k\eta, 1, \mathrm{i}\alpha c(c - u\omega)/ku\eta]_0^{\mathrm{T}}, \\ \boldsymbol{r}_2 &= [-\mathrm{i}u\alpha(c + u\omega)/c\eta k, \mathrm{i}\alpha(u + c\omega)/k\eta, 1, \mathrm{i}\alpha c(c + u\omega)/ku\eta]_0^{\mathrm{T}}, \\ \boldsymbol{r}_3 &= [1, 0, 0, 0]^{\mathrm{T}}, \quad \boldsymbol{r}_4 = [0, \mathrm{i}ku/\alpha, 1, 0]_0^{\mathrm{T}}. \end{aligned}\right\} \tag{5.14}$$

The solution components corresponding to λ_1 and λ_2 represent the propagation of pressure waves in directions toward, and away from, the rear of the reaction zone respectively along the forward and backward facing $\mathrm{d}x/\mathrm{d}t = u \pm c$ characteristics in the steady wave. The solution components corresponding to λ_3 and λ_4 are associated with entropy and vorticity variations that occur along particle paths.

When $\mathrm{Re}(\alpha) > 0$, i.e. for unstable modes, $\mathrm{Re}(\lambda_1) < 0$, while $\mathrm{Re}(\lambda_2)$, $\mathrm{Re}(\lambda_3)$ and $\mathrm{Re}(\lambda_4)$ are all positive. Consequently, as $x \to -\infty$, the mode corresponding to r_1 is spatially unbounded and must be eliminated. This is achieved by multiplying (5.13) by the left eigenvector corresponding to λ_1, and setting the result to zero. This gives

$$u' - \frac{u_0\omega}{c_0}p' - \frac{\mathrm{i}ku_0}{\alpha}w' = 0, \tag{5.15}$$

which is the required boundedness condition when $\mathrm{Re}(\alpha) > 0$. Since the mode corresponding to λ_1 describes the propagation of acoustic signals from the equilibrium zone into the rear of the reaction zone, the condition (5.15) is equivalent to having a zero-amplitude signal along all the reaction zone-facing characteristics, i.e. it is an acoustic radiation condition. For neutrally stable modes, $\mathrm{Re}(\alpha) = 0$, the mode corresponding to λ_1 is now spatially bounded at $x = -\infty$, as are the modes

corresponding to λ_2, λ_3 and λ_4. In this case, no boundedness condition can be applied. However, the condition to be applied in this case is again the elimination of the mode corresponding to λ_1, based on the causality principle that the instability of the detonation wave structure should not be influenced by waves propagating upstream from infinity. Consequently the condition that is applied for $\mathrm{Re}(\alpha)=0$ is again (5.15). For $\mathrm{Re}(\alpha)\geqslant 0$, (5.15) is applied at $\beta=0$. Of course, the condition (5.15) is that imposed by D'yakov (1954) and Kontorovich (1957) in the normal-mode examination of the stability of an inert step shock for $\mathrm{Re}(\alpha)\geqslant 0$.

5.3. *Analysis for* $\nu=1/2$

5.3.1. *Chapman–Jouguet* $f=1$

For a square-root depletion order and for Chapman–Jouguet detonations, we have $\eta=O(\beta)$ and $W=O(1)$ as $\beta\to 0$. The system (4.7) may then be written as

$$\beta z'_{,\beta}=\tilde{\boldsymbol{A}}z'+\tilde{\boldsymbol{s}},\quad \tilde{\boldsymbol{A}}=\sum_{i=0}^{\infty}\beta^i\tilde{\boldsymbol{A}}_i,\quad \tilde{\boldsymbol{s}}=\sum_{i=0}^{\infty}\beta^i\tilde{\boldsymbol{s}}_i, \tag{5.16}$$

where each of the $\tilde{\boldsymbol{A}}_i$ and $\tilde{\boldsymbol{s}}_i$ are $O(1)$ matrices, independent of β. Thus $\beta=0$ is a regular singular point of (5.16), and solutions can be obtained in a standard fashion (Wasow 2002). The five independent homogeneous solutions take the form

$$z'_{hi}\sim \boldsymbol{r}_{0i}+O(\beta), i=1,2,3,4;\quad z'_{h5}\sim \beta^{\lambda_5}(\boldsymbol{r}_{05}+O(\beta)); \tag{5.17}$$

as $\beta\to 0$, with right eigenvectors

$$\left.\begin{aligned} r_{01}=[-\alpha_2/\alpha_1,1,0,0,0]^{\mathrm{T}},\quad r_{02}=[-\alpha_3/\alpha_1,0,1,0,0]^{\mathrm{T}},\quad r_{03}=[-\alpha_4/\alpha_1,0,0,1,0]^{\mathrm{T}},\\ r_{04}=[-\alpha_5/\alpha_1,0,0,0,1]^{\mathrm{T}},\quad r_{05}=[-1,1,0,1,0]^{\mathrm{T}},\end{aligned}\right\} \tag{5.18}$$

where

$$\left.\begin{aligned} \alpha_1=\frac{u_0u_1}{\tilde{\eta}_0},\quad \alpha_2=\frac{u_0}{\tilde{\eta}_0}\left(\frac{\alpha u_0}{\widetilde{W}_0}+2u_1\right),\quad \alpha_3=-\frac{\mathrm{i}ku_0^3}{\tilde{\eta}_0\widetilde{W}_0},\\ \alpha_4=\frac{u_0}{\tilde{\eta}_0}\left(\frac{\alpha u_0}{\widetilde{W}_0}+\gamma u_1\right),\quad \alpha_5=-2Q(\gamma-1)\frac{u_0}{\tilde{\eta}_0}.\end{aligned}\right\} \tag{5.19}$$

A particular integral can be found in the form

$$z'_p\sim z'_{p0}+O(\beta),\ z'_{p0}=[2\alpha u_1u_0/\tilde{\eta}_0\lambda_5,\ -2\alpha u_1u_0/\tilde{\eta}_0\lambda_5,0,\ -2\alpha u_1u_0/\tilde{\eta}_0\lambda_5,0]^{\mathrm{T}}. \tag{5.20}$$

The eigenvalue λ_5 appearing in z'_{h5} is given by

$$\lambda_5=-1-\frac{2\alpha u_0}{(1-\delta)\widetilde{W}_0}, \tag{5.21}$$

and since $0\leqslant\delta<1$, $u_0<0$ and $\widetilde{W}_0<0$, we have that $\mathrm{Re}(\lambda_5)<0$ wherever $\mathrm{Re}(\alpha)>-(1-\delta)\widetilde{W}_0/2u_0(<0)$. Consequently, for neutrally stable or unstable modes, i.e. with $\mathrm{Re}(\alpha)\geqslant 0$, the mode z'_{h5} is spatially unbounded as $\beta\to 0$, while the modes z'_{hi}, $i=1..4$, are spatially bounded as $\beta\to 0$, each limiting to a finite amplitude. Eliminating the spatially unbounded mode z'_{h5} from the system (5.8) by setting $C_5=0$ results in the leading-order compatibility relation

$$u'+p'-\frac{\mathrm{i}ku_0}{\alpha}w'-2Q(\gamma-1)\frac{\widetilde{W}_0}{\alpha u_0}\beta'+\frac{\widetilde{W}_0u_1}{\alpha u_0}(v'+2(u'-\alpha)+\gamma p')+O(\beta)=0, \tag{5.22}$$

between the components of z', that ensures only spatially bounded solutions are present as $\beta \to 0$. The correction terms are of size $O(\beta)$ as determined from (5.17). The last two terms proportional to $\widetilde{W}_0$ that appear on the left-hand side of (5.22) are a manifestation of the finite gradient $u_{,x}$ of the steady wave solution at the end of the reaction zone (see § 3).

5.3.2. *Overdriven* $f > 1$

For the overdriven case ($f > 1$) with square-root depletion, $\eta = O(1)$ and $W = O(1)$ as $\beta \to 0$, and the system (4.7) may be written as

$$z'_{,\beta} = \tilde{\boldsymbol{A}} z' + \tilde{\boldsymbol{s}}, \quad \tilde{\boldsymbol{A}} = \sum_{i=0}^{\infty} \beta^i \tilde{\boldsymbol{A}}_i, \quad \tilde{\boldsymbol{s}} = \sum_{i=0}^{\infty} \beta^i \tilde{\boldsymbol{s}}_i. \tag{5.23}$$

Thus $\beta = 0$ is an ordinary point of the system (5.23), and solutions may be obtained in a positive integer power series form. In this case, we apply the condition (5.15) at $\beta = 0$ for $\mathrm{Re}(\alpha) \geqslant 0$ as discussed in § 5.2.

5.4. $1/2 < \nu < 1$

5.4.1. *Chapman–Jouguet* $f = 1$

For depletion orders in the range $1/2 < \nu < 1$ and for Chapman–Jouguet waves, $\eta = O(\beta)$ and $W = O(\beta^{2\nu-1})$, and the system (4.7) may be expanded in the form

$$\beta^{2\nu} z'_{,\beta} = \tilde{\boldsymbol{A}} z' + \beta^{2\nu-1} \tilde{\boldsymbol{s}}, \quad \tilde{\boldsymbol{A}} \sim \tilde{\boldsymbol{A}}_0 + \beta^{2\nu-1} \tilde{\boldsymbol{A}}_1 + \beta \tilde{\boldsymbol{A}}_2, \quad \tilde{\boldsymbol{s}} \sim \tilde{\boldsymbol{s}}_0 + \beta \tilde{\boldsymbol{s}}_1, \tag{5.24}$$

as $\beta \to 0$. Thus $\beta = 0$ is an irregular singular point of (5.24). The homogeneous solutions have the asymptotic form

$$\left.\begin{aligned} z'_{hi} &= \boldsymbol{r}_{0i} + O(\beta^{2\nu-1}, \beta^{2-2\nu}), \quad i = 1, 2, 3, \\ z'_{h4} &= \beta^{2\nu-1}(\boldsymbol{r}_{04} + O(\beta^{2\nu-1}, \beta^{2-2\nu})), \\ z'_{h5} &= \tfrac{1}{\beta} \mathrm{e}^{\lambda_5/\beta^{2\nu-1}}(\boldsymbol{r}_{05} + O(\beta^{2\nu-1}, \beta^{2-2\nu})), \end{aligned}\right\} \tag{5.25}$$

where

$$\begin{gathered} r_{01} = [1, 0, 0, 0, 0]^{\mathrm{T}}, \quad r_{02} = [0, 1, 0, -1, 0]^{\mathrm{T}}, \quad r_{03} = \left[0, 1, \frac{2\alpha}{\mathrm{i}ku_0}, 1, 0\right]^{\mathrm{T}}, \\ r_{04} = [0, 0, 0, 0, 1]^{\mathrm{T}}, \quad r_{05} = [-1, 1, 0, 1, 0]^{\mathrm{T}}. \end{gathered} \tag{5.26}$$

The size of the correction terms in (5.25) depend on whether $1/2 < \nu < 3/4$, or $3/4 < \nu < 1$. A particular integral is

$$z'_p = \beta^{2\nu-1}([-u_1 \widetilde{W}_0/u_0,\ u_1 \widetilde{W}_0/u_0, 0, u_1 \widetilde{W}_0/u_0, , 0]^{\mathrm{T}} + O(\beta^{2\nu-1}, \beta^{2-2\nu})). \tag{5.27}$$

The eigenvalue λ_5 is given by

$$\lambda_5 = 2\alpha u_0^2 / \widetilde{W}_0 \tilde{\eta}_0 (2\nu - 1), \tag{5.28}$$

so that $\mathrm{Re}(\lambda_5) > 0$ when $\mathrm{Re}(\alpha) > 0$. Consequently, for unstable modes, with $\mathrm{Re}(\alpha) > 0$, the mode z'_{h5} is spatially unbounded as $\beta \to 0$. For $\mathrm{Re}(\alpha) = 0$, the mode z'_{h5} remains spatially unbounded as $\beta \to 0$, but algebraically so. The modes z'_{hi}, $i = 1..4$, remain bounded for $\mathrm{Re}(\alpha) \geqslant 0$, but in this case modes z'_{hi}, $i = 1..3$, limit to finite amplitudes as $\beta \to 0$, whereas z'_{h4} vanishes. Eliminating the mode z'_{h5} by setting $C_5 = 0$ in (5.8)

results in the leading-order compatibility relation

$$u' + p' - \frac{\mathrm{i}ku_0}{\alpha} w' + O(\beta^{2\nu-1}, \beta^{2-2\nu}) = 0, \tag{5.29}$$

between the components of z', that ensures only spatially bounded solutions exist as $\beta \to 0$. In this case, it is of interest to write the $O(\beta^{2\nu-1})$ correction terms explicitly for $1/2 < \nu < 3/4$, so that (5.29) becomes

$$u' + p' \; -\frac{\mathrm{i}ku_0}{\alpha} w' + \beta^{2\nu-1}\left[\frac{\widetilde{W}_0 u_1}{\alpha u_0}\left(v' - 2\alpha \right.\right. \\ \left.\left. + \frac{(3-\gamma)}{2} u' + \frac{(\gamma-1)}{2} p' + \mathrm{i}k\frac{(\gamma+1)}{2\alpha} u_0 w'\right)\right] + o(\beta^{2\nu-1}) = 0. \tag{5.30}$$

As $\nu \to 1/2$, the correction terms increase in importance, enabling a smooth matching with the boundedness condition for $\nu = 1/2$ (5.22).

5.4.2. *Overdriven* $f > 1$

For the overdriven case with a depletion order in the range $1/2 < \nu < 1$, $\eta = O(1)$ and $W = O(\beta^{2\nu-1})$, and the system (4.7) may be expanded as

$$\beta z'_{,\beta} = \tilde{\boldsymbol{A}} z' + \beta \tilde{\boldsymbol{s}}, \quad \tilde{\boldsymbol{A}} \sim \tilde{\boldsymbol{A}}_0 + \beta^{2-2\nu}\tilde{\boldsymbol{A}}_1 + \beta\tilde{\boldsymbol{A}}_2, \quad \tilde{\boldsymbol{s}} \sim \tilde{\boldsymbol{s}}_0 + \beta\tilde{\boldsymbol{s}}_1. \tag{5.31}$$

Nominally it appears that $\beta = 0$ is a regular singular point of (5.31). However, the homogeneous solutions take the form

$$z'_{hi} \sim \boldsymbol{r}_{0i} + O(\beta^{2-2\nu}), \quad i = 1, 2, 3, 4; \quad z'_{h5} \sim \boldsymbol{r}_{05}\beta^{2\nu-1} + O(\beta), \tag{5.32}$$

where

$$\left.\begin{aligned} r_{01} = [1, 0, 0, 0, 0]^{\mathrm{T}}, \quad r_{02} = [0, 1, 0, 0, 0]^{\mathrm{T}}, \quad r_{03} = [0, 0, 1, 0, 0]^{\mathrm{T}}, \\ r_{04} = [0, 0, 0, 1, 0]^{\mathrm{T}}, \quad r_{05} = [0, 0, 0, 0, 1]^{\mathrm{T}}. \end{aligned}\right\} \tag{5.33}$$

A particular integral can be obtained in the form

$$z'_p = \beta\left([0, 0, 0, 0, \alpha/u_0]^{\mathrm{T}}/(2-2\nu) + O(\beta^{2\nu-1,2-2\nu})\right). \tag{5.34}$$

Thus all the solution components are in fact spatially bounded as $\beta \to 0$, and thus the apparent singularity in (5.31) was removable. In this case, we again apply the condition (5.15) at $\beta = 0$ for $\mathrm{Re}(\alpha) \geqslant 0$.

5.5. $\nu = 1$

5.5.1. *Chapman–Jouguet* $f = 1$

For simple depletion ($\nu = 1$) and Chapman–Jouguet waves ($f = 1$), $\eta = O(\beta)$, $W = O(\beta)$, and the system (4.7) may be expanded in the form

$$\beta^2 z'_{\beta} = \tilde{\boldsymbol{A}} z' + \beta\tilde{\boldsymbol{s}}, \quad \tilde{\boldsymbol{A}} = \sum_{i=0}^{\infty} \beta^i \tilde{\boldsymbol{A}}_i, \quad \tilde{\boldsymbol{s}} = \sum_{i=0}^{\infty} \beta^i \tilde{\boldsymbol{s}}_i, \tag{5.35}$$

as $\beta \to 0$. Thus $\beta = 0$ is an irregular singular point of (5.35). The homogeneous solutions take the asymptotic form

$$\left.\begin{aligned} z'_{h1} &\sim \beta^{-\alpha/\widetilde{W}_0}(\boldsymbol{r}_{01} + O(\beta)) + c_1\beta^{1-\alpha/\widetilde{W}_0}\log\beta\,(\boldsymbol{r}_{11} + O(\beta)), \\ z'_{h2} &\sim \beta^{\lambda_1}(\boldsymbol{r}_{02} + O(\beta)), \\ z'_{h3} &\sim \beta^{-\alpha/\widetilde{W}_0}(\boldsymbol{r}_{03} + O(\beta)) + c_2\beta^{1-\alpha/\widetilde{W}_0}\log\beta\,(\boldsymbol{r}_{13} + O(\beta)), \\ z'_{h4} &\sim \beta^{1-\alpha/\widetilde{W}_0}(\boldsymbol{r}_{04} + O(\beta)), \quad z'_{h5} \sim \beta^d \mathrm{e}^{\lambda_2/\beta}(\boldsymbol{r}_{05} + O(\beta)), \end{aligned}\right\} \tag{5.36}$$

as $\beta \to 0$, where the right eigenvectors are

$$\begin{gathered} r_{01} = [1, 0, 0, 0, 0]^{\mathrm{T}}, \quad r_{02} = [a + b, a - b, 2\mathrm{i}\alpha b/u_0 k, -a - b, 0]^{\mathrm{T}}, \\ r_{03} = [0, 1, -\mathrm{i}\alpha/u_0 k, 0, 0]^{\mathrm{T}}, \quad r_{04} = r_{11} = r_{13} = [0, 0, 0, 0, 1]^{\mathrm{T}}, \quad r_{05} = [1, -1, 0, -1, 0]^{\mathrm{T}}, \end{gathered} \tag{5.37}$$

with

$$\left.\begin{gathered} a = -\alpha/\widetilde{W}_0, \quad b = -u_0^2 k^2/2\alpha, \quad c_1 = \theta/u_0^2 p_0, \quad c_2 = -1/u_0, \\ d = -1 + \frac{4\alpha^2 u_0 \widetilde{W}_1 - \widetilde{W}_0 u_1(\alpha^2(3-\gamma) - k^2 u_0^2(\gamma+1))}{2(\gamma+1)u_1 \widetilde{W}_0^2 \alpha}. \end{gathered}\right\} \tag{5.38}$$

A particular integral can be found in the form

$$z'_p = \beta[-u_1\widetilde{W}_0/u_0,\ u_1\widetilde{W}_0/u_0, 0, u_1\widetilde{W}_0/u_0,\ , 0]^{\mathrm{T}} + O(\beta^2). \tag{5.39}$$

The eigenvalues λ_1 and λ_2 are given by

$$\lambda_1 = -\left(\alpha^2 + u_0^2 k^2\right)/2\alpha\widetilde{W}_0, \quad \lambda_2 = 2\alpha u_0^2/\widetilde{W}_0\tilde{\eta}_0, \tag{5.40}$$

so that for $\mathrm{Re}(\alpha) > 0$, $\mathrm{Re}(\lambda_1) > 0$ and $\mathrm{Re}(\lambda_2) > 0$. For $\mathrm{Re}(\alpha) = 0$, $\mathrm{Re}(d) < 0$, and consequently only the mode z'_{h5} is unbounded as $\beta \to 0$ for $\mathrm{Re}(\alpha) \geqslant 0$. Modes z'_{hi}, $i = 1..4$, all vanish as $\beta \to 0$ for $\mathrm{Re}(\alpha) > 0$, while modes z'_{h1} and z'_{h3} remain finite as $\beta \to 0$ for $\mathrm{Re}(\alpha) = 0$. Upon elimination of the mode z'_{h5}, by setting $C_5 = 0$ in (5.8), we arrive at the compatibility condition

$$u' + p' - \frac{\mathrm{i}ku_0}{\alpha}w' + O(\beta\log\beta^{-1}) = 0, \tag{5.41}$$

that ensures spatially bounded eigenfunction solutions as $\beta \to 0$.

5.5.2. *Overdriven* $f > 1$

For simple depletion, $\nu = 1$, and overdriven waves, $\eta = O(1)$ and $W = O(\beta)$. The system (4.7) can then be expanded as

$$\beta z'_\beta = \tilde{\boldsymbol{A}}\boldsymbol{z}' + \beta\tilde{\boldsymbol{s}}, \quad \tilde{\boldsymbol{A}} = \sum_{i=0}^{\infty}\beta^i\tilde{\boldsymbol{A}}_i, \quad \tilde{\boldsymbol{s}} = \sum_{i=0}^{\infty}\beta^i\tilde{\boldsymbol{s}}_i, \tag{5.42}$$

as $\beta \to 0$. Thus $\beta = 0$ is a regular singular point of (5.42). The homogeneous solutions take the form

$$\left.\begin{aligned} z'_{h1} &= \beta^{-\alpha/\widetilde{W}_0}(\boldsymbol{r}_{01} + O(\beta)) + c_1\beta^{1-\alpha/\widetilde{W}_0}\log\beta\,(\boldsymbol{r}_{11} + O(\beta)), \\ z'_{h2} &= \beta^{-\alpha/\widetilde{W}_0}(\boldsymbol{r}_{02} + O(\beta)) + c_2\beta^{1-\alpha/\widetilde{W}_0}\log\beta\,(\boldsymbol{r}_{12} + O(\beta)), \\ z'_{h3} &= \beta^{1-\alpha/\widetilde{W}_0}(\boldsymbol{r}_{03} + O(\beta)), \quad z'_{hi} \sim \boldsymbol{r}_{0i}\beta^{\lambda_i} + O(\beta),\ i = 4, 5, \end{aligned}\right\} \tag{5.43}$$

as $\beta \to 0$, where the right eigenvectors r_{01}, r_{02} and r_{03} are

$$r_{01} = [1, 0, 0, 0, 0]^{\mathrm{T}}, \quad r_{03} = r_{11} = r_{12} = [0, 0, 0, 0, 1]^{\mathrm{T}}, \quad r_{02} = [0, 1, -\mathrm{i}\alpha/u_0 k, 0, 0]^{\mathrm{T}}, \tag{5.44}$$

and where the eigenvectors $\boldsymbol{r}_{04}$ and $\boldsymbol{r}_{05}$, and the constants c_1 and c_2, can be obtained in terms of the ZND state. A particular integral can be found in the form

$$z'_p = \beta[0, 0, 0, 0, \widetilde{W}_0/u_0]^{\mathrm{T}} + O(\beta^2). \tag{5.45}$$

The eigenvalues λ_4 and λ_5 are given by

$$\lambda_4 = -\frac{u_0\alpha}{\eta_0\widetilde{W}_0}(u_0 + c_0\omega), \quad \lambda_5 = -\frac{u_0\alpha}{\eta_0\widetilde{W}_0}(u_0 - c_0\omega), \quad \omega = \sqrt{1 - \eta_0 k^2/\alpha^2}, \tag{5.46}$$

so that for $\mathrm{Re}(\alpha) > 0$, $\mathrm{Re}(\lambda_4) > 0$ and $\mathrm{Re}(\lambda_5) < 0$. Consequently only the mode z'_{h5} is unbounded at $\beta = 0$ for $\mathrm{Re}(\alpha) > 0$. Upon elimination of this mode, we arrive at the compatibility condition

$$u' - \frac{u_0\omega}{c_0}p' - \frac{\mathrm{i}ku_0}{\alpha}v' + O(\beta\log\beta^{-1}) = 0, \tag{5.47}$$

that ensures spatially bounded eigenfunction solutions as $\beta \to 0$ for $\mathrm{Re}(\alpha) > 0$. Modes z'_{hi}, $i = 1..4$, again all vanish as $\beta \to 0$ for $\mathrm{Re}(\alpha) > 0$. For $\mathrm{Re}(\alpha) = 0$, the mode z'_{h5} is now spatially bounded along with the modes z'_{hi}, $i = 1..4$, and no boundedness condition can be applied. For consistency, we impose the radiation condition (5.15) that eliminates upstream propagating waves at the point $\beta = 0$.

5.6. *Boundedness conditions for Chapman–Jouguet waves revisited*

Further insights into the origin of the single spatially unbounded mode found for Chapman–Jouguet waves can be obtained by extracting from the system (2.1)–(2.8) an equation which describes any forward travelling plane wave in the x-direction (Roe 1998). When specialized to the shock frame (4.1), this is

$$\begin{aligned} p_{,t} + (u + c)p_{,x} + c\rho(u_{,t} + (u + c)u_{,x}) &= \Psi_{,t}(p_{,x} + c\rho u_{,x}) - c\rho w(u_{,z} - \Psi_{,z}u_{,x}) \\ &\quad - w(p_{,z} - \Psi_{,z}p_{,x}) - c^2\rho(w_{,z} - \Psi_{,z}w_{,x}) - 2(\gamma - 1)\beta\rho Q W. \end{aligned} \tag{5.48}$$

Linearizing according to (4.3) and (4.5) and employing the coordinate transformation (4.6) gives, at $O(\epsilon)$,

$$\begin{aligned} W\left(1 + \frac{c}{u}\right)(p'_{,\beta} + c\rho u'_{,\beta}) &= -\alpha(p' + c\rho u') - \frac{W}{u}(u' + c' - \alpha)(p_{,\beta} + c\rho u_{,\beta}) \\ &\quad - (c'\rho + \rho' c)\left(1 + \frac{c}{u}\right)W u_{,\beta} - \mathrm{i}kc^2\rho w' - 2(\gamma - 1)QW(\beta'\rho + \beta\rho') \\ &\quad - 2(\gamma - 1)\beta\rho Q(W_{,p}p' + W_{,v}v' + W_{,\beta}\beta'), \end{aligned} \tag{5.49}$$

which describes the behaviour of the perturbations along any forward acoustic characteristic defined by the steady wave solution when $0 \leqslant \beta \leqslant 1$. Note that the coefficient of the derivative term on the left-hand side of (5.49) vanishes for the Chapman–Jouguet wave since $c \to -u$ as $\beta \to 0$. It is easy to demonstrate, from the solutions developed in § 5.3.1, § 5.4.1 and § 5.5.1, that the left-hand side of (5.49) vanishes for each of the spatially bounded modes (i.e. those in (5.17), (5.25) and (5.36)). It is also easy to demonstrate that the single unbounded mode calculated in each of (5.17), (5.25) and (5.36) as $\beta \to 0$ has its origin in the vanishing of the coefficient on the left-hand side of (5.49). Thus, given our prior knowledge of the spatial structure of the modal solutions determined in § 5.3.1, § 5.4.1 and § 5.5.1, the boundedness condition for each case could be simply derived by setting the left-hand side of (5.49) to zero as $\beta \to 0$, where $u \to -c$. This gives, to leading-order,

$$p' + u' - \frac{\mathrm{i}ku_0}{\alpha} w' - 2Q(\gamma - 1)\frac{\widetilde{W}_0}{\alpha u_0}\beta' + \frac{\widetilde{W}_0 u_{,\beta}}{\alpha u_0}(v' + \gamma p' + 2(u' - \alpha)) = 0, \qquad (5.50)$$

which coincides with the leading-order conditions (5.22), (5.29) and (5.41) for the appropriate ν in the range $1/2 \leqslant \nu \leqslant 1$. Comments regarding the appropriateness of linearization of the flow equations around a sonic flow point are given in § 6.

5.7. *Evaluation of* α

The eigenvalue α, for a given parameter set, is formally obtained by the integral solution of (4.7) that satisfies the shock conditions (4.11) at $\beta = 1$ and, depending on the parameter values of f and ν, one of the above boundedness conditions (or radiation condition in the case of $f > 1$, $1/2 \leqslant \nu \leqslant 1$, $\mathrm{Re}(\alpha) = 0$) as $\beta \to 0$. In practice, this is done by a shooting algorithm, similar, for example, to that described in Short & Stewart (1998). For the calculations shown in § 6, the leading-order boundedness conditions are typically applied at $\beta = 10^{-7}$. For this small value of β, further decreases in β are found to not change α at the accuracy calculated for the present paper (see tables 1 and 2). To summarize, the boundedness condition for $f = 1$, $\nu = 1/2$, is given by (5.22), provided $\mathrm{Re}(\alpha) > -(1 - \delta)\widetilde{W}_0/2u_0 (< 0)$; by (5.29) for $f = 1$, $1/2 < \nu < 1$, provided $\mathrm{Re}(\alpha) \geqslant 0$; by (5.41) for $f = 1$, $\nu = 1$, provided $\mathrm{Re}(\alpha) \geqslant 0$; by (5.47) for $f > 1$, $\nu = 1$, provided $\mathrm{Re}(\alpha) > 0$; and by (5.15) for $f > 1$, $1/2 \leqslant \nu < 1$ for $\mathrm{Re}(\alpha) > 0$. The radiation condition that is applied for $f > 1$, $1/2 \leqslant \nu \leqslant 1$ for $\mathrm{Re}(\alpha) = 0$ is given by (5.15).

6. Additional comments on the linear stability analysis

6.1. *Influence of the transonic layer for Chapman–Jouguet waves*

In this section, we address questions concerning the validity of the linearization of unsteady flow perturbations in a transonic flow region for the case of Chapman–Jouguet detonations. First, we recall the premise behind our analysis: this involves an $O(\epsilon)$ perturbation uniformly applied to the steady detonation structure (4.3). Secondly, we recognize that the structure of a CJ detonation can be characterized by two smoothly merging flow regimes: a main reaction layer (or MRL), where most of heat is released, and a transonic layer (or TSL), where the flow is near-sonic (Klein 1991). The main reaction layer is defined as the region where $\beta = O(1)$, while, for reasons noted below, the transonic layer is defined as the region where $\beta = O(\epsilon)$. The potential problem with the linear approximation lies with the long-time shape of the upstream acoustic wave characteristic paths initially in the region $\beta = O(\epsilon)$. For example, the upstream characteristic through $\beta = 0$, i.e. through the steady sonic point, remains at $\beta = 0$ in the linear approximation. In practice, we should expect

that accumulative nonlinear effects on an appropriately defined time scale in the transonic layer will modify the shape of the characteristics in the region $\beta = O(\epsilon)$ by an $O(\epsilon)$ amount. We will now obtain the time scale for the breakdown of the linear approximation in the transonic layer, and discuss the implications for a linear stability analysis.

The time scales that characterize the unsteady evolution in the transonic and main reaction layers can be extracted from a scaling argument similar to that given in Klein (1991) and Bdzil *et al.* (2006) (upon omitting the curvature terms). The characteristic width of the two regions is defined by the distance a reacting particle would travel in each region over the change in reactant mass fraction. Since the main reaction layer is the region defined for $\beta = O(1)$, the fluid velocity (3.1) is $O(1)$ based on the dimensional scales defined in § 2, while the reaction rate $W = O(1)$, the characteristic MRL length scale is

$$l_{\mathrm{MRL}} = O\left(\frac{\beta}{W}u\right) = O(1). \tag{6.1}$$

Consequently, given that the three characteristic (particle u, upstream $u + c$, and downstream acoustic $u - c$) velocities are $O(1)$ as defined by the scales in § 2, the MRL time scale is

$$t_{\mathrm{MRL}} = O(1). \tag{6.2}$$

Thus, it is important to recognize that the time scale t associated with the linearization (4.3) is that of the characteristic time scale of the evolution of disturbances in the main reaction layer. For the transonic layer, an examination of (5.48) shows that an $O(\epsilon)$ disturbance has the ability to influence the leading-order path of the upstream, near-sonic characteristics in a region where $\beta = O(\epsilon)$. This is the region we define as the transonic layer. Since the flow velocity in the TSL is $O(1)$ through (5.1), while $W = O(\epsilon^{2\nu-1})$ (see (5.7)), the characteristic length scale of the transonic layer is

$$l_{\mathrm{TSL}} = O\left(\frac{\beta}{W}u\right) = O(\epsilon^{2-2\nu}). \tag{6.3}$$

In the TSL, both the flow velocity u and downstream acoustic wave speed $u - c$ are $O(1)$. Thus the time scale associated with the movement of these two wave families through the transonic layer is then $O(\epsilon^{2-2\nu})$. On the other hand, in the region where $\beta = O(\epsilon)$, the upstream acoustic wave speed in the TSL is $u + c = O(\epsilon)$. Thus the time scale associated with the motion of forward acoustic wave disturbances through the transonic layer is

$$t_{\mathrm{TSL}} = O(\epsilon^{1-2\nu}). \tag{6.4}$$

It is the nonlinear TSL evolution on the time scale t_{TSL} that is relevant to our problem.

The relevant length and time scales in the MRL and TSL can now be compared for a reaction order in the range $1/2 \leqslant \nu \leqslant 1$. We first note that $t_{\mathrm{TSL}}/t_{\mathrm{MRL}} = O(\epsilon^{1-2\nu})$, so that $t_{\mathrm{TSL}}/t_{\mathrm{MRL}} \gg 1$ for a reaction order in the range $1/2 < \nu \leqslant 1$, while $t_{\mathrm{TSL}}/t_{\mathrm{MRL}} = O(1)$ for $\nu = 1/2$. For the length scales, $l_{\mathrm{TSL}}/l_{\mathrm{MRL}} = O(\epsilon^{2-2\nu})$, so that $l_{\mathrm{TSL}}/l_{\mathrm{MRL}} \ll 1$ for $1/2 \leqslant \nu < 1$, while $l_{\mathrm{TSL}}/l_{\mathrm{MRL}} = O(1)$ for $\nu = 1$. Consequently, a formal analysis of the transonic layer evolution would require introduction of the scales

$$\hat{t} = \epsilon^{2\nu-1}t, \quad \hat{x} = \epsilon^{2\nu-2}x, \quad \hat{\beta} = \epsilon^{-1}\beta, \tag{6.5}$$

combined with the perturbation expansion (4.3). The nonlinear evolution along the forward characteristic in the TSL can be obtained from (5.48) and is defined

by

$$\bar{p}_{,\hat{t}} + \bar{u}_{,\hat{t}} + \left(\frac{\hat{\beta}}{2} + \bar{u} + \bar{c}\right)\left[\bar{p}_{,\hat{x}} + \bar{u}_{,\hat{x}} - 2\frac{\widetilde{W}_0}{\gamma}\hat{\beta}^{2\nu-1}\right] = -\frac{\widetilde{W}_0}{\gamma}\hat{\beta}^{2\nu-1}[\hat{\beta} + (2\nu-1)\bar{\beta}]$$
$$+\epsilon^{2\nu-1}\bar{\Psi}_{,\hat{t}}\left[\bar{p}_{,\hat{x}} + \bar{u}_{,\hat{x}} - 2\frac{\widetilde{W}_0}{\gamma}\hat{\beta}^{2\nu-1}\right] - \epsilon^{2-2\nu}\frac{\gamma}{(\gamma+1)}\left[\frac{\bar{w}_{,z}}{\epsilon} - \epsilon^{2\nu-2}\bar{\Psi}_{,z}\bar{w}_{,\hat{x}}\right]$$
$$-\epsilon^{2-2\nu}\bar{w}\left[\bar{p}_{,z} + \bar{u}_{,z} - \bar{\Psi}_{,z}\epsilon^{2\nu-1}\left(\bar{p}_{,\hat{x}} + \bar{u}_{,\hat{x}} - 2\frac{\widetilde{W}_0}{\gamma}\hat{\beta}^{2\nu-1}\right)\right]. \tag{6.6}$$

Several comments can now be made regarding the role of the transonic layer in the linear stability analysis. For a reaction order in the range $1/2 < \nu \leqslant 1$, $t_{\mathrm{TSL}} \gg t_{\mathrm{MRL}}$ for $\epsilon \ll 1$, i.e. the defining disturbance evolution time in the transonic layer is much greater than that in the main reaction layer. Thus, on the shorter main reaction layer time scale, the linear analysis described in § 4 and § 5 for $f = 1$ is valid for the transonic layer $\beta = O(\epsilon)$. In particular, this implies that if the detonation is unstable ($\mathrm{Re}(\alpha) > 0$) on the MRL time scale, as for the cases shown in § 7, the TSL cannot influence this outcome. The only potential source of difficulty occurs for square-root depletion, $\nu = 1/2$, where $t_{\mathrm{TSL}} = O(t_{\mathrm{MRL}})$. For the MRL region $O(\epsilon) < \beta \leqslant 1$, $\epsilon \to 0$, the linear analysis in § 4 and § 5 remains valid. In particular, the spatial growth of the mode z'_{h5} (5.17) is unbounded ($z'_{h5} \sim \boldsymbol{r}_{05}\beta^{\lambda_5}$, $\lambda_5 = -1 - 2\alpha u_0/(1-\delta)\widetilde{W}_0$) as $\beta \to 0$. Based on the analysis in Klein (1991) and Bdzil *et al.* (2006), we surmise that an $O(\epsilon)$ disturbance in the nonlinear TSL (where $\beta = O(\epsilon)$) cannot be matched to the unbounded spatial growth of the eigenfunction z'_{h5} in the MRL. Consequently, the boundedness condition (5.22) must still be applied at the end of the MRL, where $\beta = O(\epsilon)$, making the disturbances uniformly of size $O(\epsilon)$ at the end of MRL. Most importantly, this condition completely isolates the linear evolution of the MRL from the TSL, so that the influence of the TSL on the MRL will be $o(\epsilon)$ as in Klein (1991) and Bdzil *et al.* (2006). In short, for $\nu = 1/2$, the TSL dynamics does not affect the linear evolution of the MRL region, and so the linear stability analysis described in § 4 and § 5 remains valid. The outstanding agreement between the numerical simulations shown in § 7 and the linear stability theory justifies this argument.

6.2. *Decay dynamics of linearly perturbed stable waves*

In the linear analysis described in § 4–5, and the calculations presented in § 7, we have only been concerned with the calculation of either neutrally stable $\mathrm{Re}(\alpha) = 0$, or unstable, $\mathrm{Re}(\alpha) > 0$, modal solutions of the exponential form (4.5). The possible existence and decay rate of modal solutions of the form (4.5) with $\mathrm{Re}(\alpha) < 0$ has not been explicitly studied. In many cases, problematic issues arise and these are highlighted below.

Modal solutions of the form (4.5) are only valid for $\mathrm{Re}(\alpha) < 0$ if they remain spatially bounded, i.e. if either the asymptotic solution (5.8) as $\beta \to 0$ or solution (5.13) as $x \to -\infty$ is spatially bounded, depending on the value of f and ν. This is the situation for $\mathrm{Re}(\alpha) \geqslant 0$ that has already been studied. We now return to each of the cases studied in § 5, and re-examine the spatial behaviour of the solution (5.8) or (5.13) for $\mathrm{Re}(\alpha) < 0$. Before proceeding, we note that for $\mathrm{Re}(\alpha) < 0$, the particular solution z'_p in (5.8) is always spatially bounded (§ 5.3–5.5), and thus only the spatial behaviour of the homogeneous terms needs to be considered.

For $f = 1$ and $\nu = 1$ (§ 5.5.1), we have that for $\mathrm{Re}(\alpha) < 0$, $\mathrm{Re}(\lambda_1) < 0$ and $\mathrm{Re}(\lambda_2) < 0$. Thus the modes z'_{hi}, $i = 1..3$, are unbounded as $\beta \to 0$ for $\mathrm{Re}(\alpha) < 0$, while the mode z'_{h4} is unbounded for $\mathrm{Re}(\alpha) < \widetilde{W}_0 (< 0)$. Only the mode z'_{h5} is bounded for

$\mathrm{Re}(\alpha) < 0$. Consequently, there will be a minimum of three modes that are spatially unbounded for $\mathrm{Re}(\alpha) < 0$. A spatially bounded form of (5.8) would then require having C_1, C_2, C_3 and possibly C_4 in (5.8) all be zero for a given eigenvalue α. This presents an overdetermined problem for α, since only one of the coefficients C_i can be eliminated for any one value of α. For $\nu = 1$ and $f > 1$ (§ 5.5.2), we have for $\mathrm{Re}(\alpha) < 0$, $\mathrm{Re}(\lambda_4) < 0$, while $\mathrm{Re}(\lambda_5) > 0$. Consequently, z'_{h1}, z'_{h2} and z'_{h4} are all spatially unbounded for $\mathrm{Re}(\alpha) < 0$ as $\beta \to 0$, z'_{h3} is unbounded for $\mathrm{Re}(\alpha) < \widetilde{W}_0$, while z'_{h5} is bounded for $\mathrm{Re}(\alpha) < 0$. As above, all of the C_i, $i = 1, 2, 4$, and possibly C_3 would need to be set to zero for (5.8) to have bounded solutions, which again represents an overdetermined system for the eigenvalue α. Consequently for $f \geqslant 1$, $\nu = 1$, as also noted by Sharpe (1997), it appears that formally there are no modal solutions of the form (4.5) with $\mathrm{Re}(\alpha) < 0$ that remain spatially bounded as $\beta \to 0$.

It should be noted, however, that attempts have been made to compare the temporal decay behaviour of a perturbed stable detonation under the idealized gas phase model with $f \geqslant 1$ and $\nu = 1$, calculated via a direct numerical simulation of (2.1)–(2.4), with an exponential modal solution of the form (4.5) (Bourlioux, *et al.* 1991*a*; Short & Blythe 2002). The boundary condition that has been applied in the linear stability analysis for $\mathrm{Re}(\alpha) < 0$ in these studies is that of no incoming acoustic modes as $\beta \to 0$, i.e. a radiation condition that equivalently sets $C_5 = 0$ in (5.8) for $f \geqslant 1$ and $\nu = 1$. Formally, the structure (5.8) then must involve spatially unbounded modes as $\beta \to 0$ (§ 5.5.1 and § 5.5.2). Nevertheless, the agreement between the $\mathrm{Re}(\alpha) < 0$ exponential decay rate evaluated from the linear analysis and that fitted to apparent exponentially decaying shock perturbation amplitudes identified in the numerical simulations was found to be excellent. One plausible explanation for this has been given by Short & Blythe (2002); the simulations are typically conducted on a finite, not infinite, domain, with a non-reflecting boundary condition applied downstream of the detonation. Formally, this prevents acoustic disturbances entering the numerical domain from downstream of the detonation, which is effectively the boundary condition applied in the linear analysis. That said, as pointed out by Bourlioux, Majda & Roytburd (1991*b*), the interpretation of α as an eigenvalue is problematic due to the unbounded spatial growth that formally exists as $\beta \to 0$ in the modal solutions (4.5).

For $f > 1$ and $1/2 \leqslant \nu < 1$, the spatial behaviour of the eigenfunction solutions in the uniform subsonic region downstream of the detonation reaction zone is given by (5.13). For $\mathrm{Re}(\alpha) < 0$, $\mathrm{Re}(\lambda_1) > 0$, but $\mathrm{Re}(\lambda_i) < 0$, $i = 1..3$. Thus only the mode corresponding to $\boldsymbol{r}_1$ in (5.13), i.e. that associated with upstream acoustic wave propagation, is spatially bounded as $x \to -\infty$, while the other three that are associated with downstream acoustic wave propagation, entropy and vorticity variations are spatially unbounded. Consequently, it again appears that formally there are no modal solutions of the form (4.5) with $\mathrm{Re}(\alpha) < 0$ that remain spatially bounded as $x \to -\infty$. In their analysis of overdriven detonations, Clavin *et al.* (1997) and Daou & Clavin (2003) choose α, with $\mathrm{Re}(\alpha) < 0$, to suppress the downstream propagating acoustic mode. This equates to setting $C_2 = 0$ in (5.13), thereby assuring that the acoustic pressure mode is bounded. However, this is also problematic as it leaves the ρ'_a, u'_a and w'_a modes spatially unbounded as $x \to -\infty$.

For $f = 1$ and $1/2 < \nu < 1$ (§ 5.4.1), we have that $\mathrm{Re}(\lambda_5) < 0$ for $\mathrm{Re}(\alpha) < 0$. In contrast to the cases discussed above, now all the modes z'_{hi}, $i = 1..5$, are spatially bounded as $\beta \to 0$ for $\mathrm{Re}(\alpha) < 0$. Since the main reaction layer perturbation solutions through (5.25) are spatially bounded, the question of the existence of exponential modal solutions of the form (4.5) would require an examination of perturbations in the attached transonic flow zone for $\beta = O(\epsilon)$, utilizing the scales identified in § 6.1. We do not pursue such an analysis here. The final case we need to examine occurs for $f = 1$

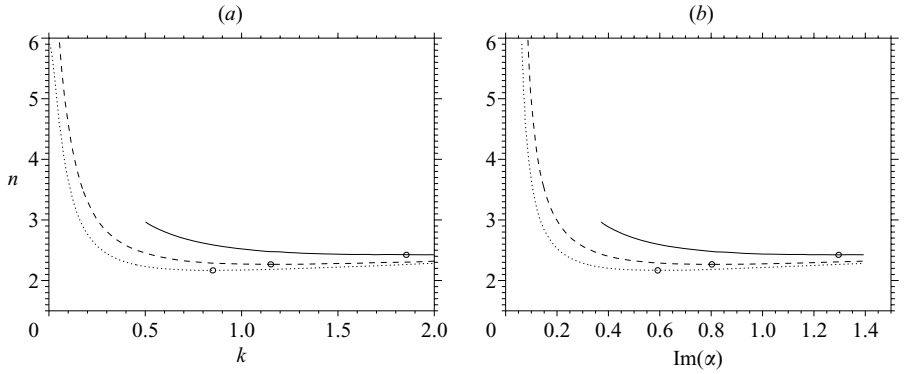

FIGURE 5. (*a*) Neutral stability boundaries in the $n-k$ plane for $k<2$ with $f=1$ when $\nu=1/2$ (dotted), $\nu=2/3$ (dashed) and $\nu=1$ (solid). Only the part for $n<3$ is calculated for $\nu=1$ due to numerical stiffness difficulties in calculating the larger-n cases. The circles mark the point of two-dimensional neutral stability in the (n,k) plane for each ν. (*b*) Corresponding frequency variation along the neutral stability boundaries over the extent shown in (*a*).

and $\nu=1/2$ (§ 5.3.1). In this case, $\mathrm{Re}(\lambda_5)<0$ for $\mathrm{Re}(\alpha)>-(1-\delta)\widetilde{W}_0/2u_0(<0)=K_p$. Thus for $\mathrm{Re}(\alpha)<K_p$, all modes z'_{hi}, $i=1..5$, are spatially bounded, as above. However, for $K_p<\mathrm{Re}(\alpha)<0$, $\mathrm{Re}(\lambda_5)<0$, and thus the mode z'_{h5} is spatially unbounded while modes z'_{hi}, $i=1..4$, are spatially bounded. Eliminating the single unbounded mode z'_{h5} as $\beta\to 0$ leads to the boundedness condition (5.22) for $K_p<\mathrm{Re}(\alpha)<0$. This is the only case for $f\geqslant 1$ and $1/2\leqslant\nu\leqslant 1$ for which the calculation of stable modal solutions of the exponential form (4.5) is not potentially problematic. A similar situation also arises in the study of the stability of pathological detonations (Sharpe 1999). It remains to suggest that for $f=1$, $1/2<\nu\leqslant 1$, and $f>1$, $1/2\leqslant\nu\leqslant 1$, the precise form of the damping behaviour of linearly perturbed detonations, and clarification on the existence of modal solutions of the form (4.5), can likely be obtained through a method of characteristics approach such as that examined for inert step-shock waves (Roberts 1945).

7. Linear stability of detonations for the idealized condensed-phase model

In the following, solutions of the above linear stability formulation for ZND detonations described by the idealized condensed-phase model are presented. Thus, unless noted otherwise, the parameter values $\theta=0$, $\delta=0$ and $\gamma=3$ will be assumed.

Figure 5 shows the neutral stability boundaries for two-dimensional perturbations to a CJ detonation in the wavenumber k and pressure sensitivity n space for three values of the depletion order $\nu=1/2$, $\nu=2/3$ and $\nu=1$. For all the CJ detonation parameter sets that have been studied, only a single unstable mode has been identified, and thus each of the boundaries shown in figure 5(*a*) is the neutral stability curve for that mode. This in contrast to our usual experience with the stability characteristics of ZND detonations defined by the idealized gas phase model, where, for example, the boundary defining detonation stability to two-dimensional disturbances in activation energy–wavenumber space is typically defined by the presence of fundamental and higher harmonic modes (e.g. Short & Stewart 1998). For one-dimensional disturbances, the CJ detonation is unstable for $n>5.904$ when $\nu=1/2$ ($\alpha_i=0.0629$), for $n>7.397$ when $\nu=2/3$ ($\alpha_i=0.0774$), and for $n>10.151$ when $\nu=1$ ($\alpha_i=0.1204$). For a value of n less than the one-dimensional neutral stability point for a given ν, there is a finite

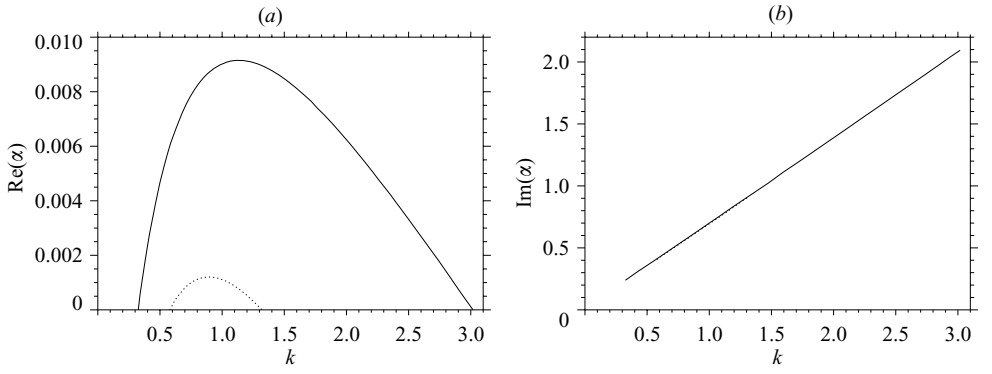

FIGURE 6. Variation of (*a*) the growth rate $\mathrm{Re}(\alpha)$ and (*b*) the frequency $\mathrm{Im}(\alpha)$ of the unstable CJ mode with k for $f=1$, $\nu=1/2$ and $n=2.2$ (dotted), $n=2.4$ (solid).

band of wavenumbers for which the detonation is unstable to transverse disturbances. The two-dimensional CJ detonation neutral stability points occur at $n=2.168$ when $\nu=1/2$ (where $k=0.851$, $\alpha_i=0.592$), at $n=2.267$ when $\nu=2/3$ (where $k=1.152$, $\alpha_i=0.803$), and at $n=2.424$ when $\nu=1$ (where $k=1.855$, $\alpha_i=1.296$). Thus decreasing the reaction order ν tends to render the ZND detonation less stable, i.e. a lower value of the pressure sensitivity exponent n is required for instability. Of particular note is that for n slightly larger than the two-dimensional neutral stability point, the band of wavenumbers for which the detonation is unstable increases rapidly. For example, when $\nu=1/2$ and $n=2.2$, this band of wavenumbers is given by $0.578<k<1.320$, whereas for $n=2.4$ the band is given by $0.325<k<3.018$. The growth rates and frequencies associated with the unstable mode when $\nu=1/2$ for $n=2.2$ and $n=2.4$ are shown in figure 6. For $n=2.4$, the maximum growth rate $\alpha_r=0.00915$ occurs at $k=1.134$ where $\alpha_i=0.791$, which translates to an initial detonation cell width $C_w=5.54$ and cell length $C_L=7.94$. Thus the initial detonation cell spacing and length are both comparable to, but smaller than, the total length $L_{\mathrm{ZND}}=8.1$ (i.e. shock to final point) of the underlying ZND wave. From a practical viewpoint, when the idealized condensed-phase detonation model is used to model real explosives, such as liquid nitromethane or solid PBX-9501, a choice of $\nu=1/2$ and a pressure sensitivity in the range $n=1-3$ is normally taken (Bdzil *et al.* 2003). In this case, a planar CJ detonation would only be stable to multi-dimensional disturbances when the pressure sensitivity $n<2.168$. We should also point out that the location of the neutral stability boundary calculated for $\nu\to1/2$ using (5.29) limits smoothly to that calculated for $\nu=1.2$ using (5.22). As noted above, the additional leading-order terms appearing in (5.22) are a simple manifestation of the change in steady structure as $\nu\to1/2$, where $u_{,x}$ and W are $O(\beta^{2\nu-1})$ as $\beta\to0$. Thus, for any $\nu>1/2$, both $u_{,x}$ and W are $o(1)$ as $\beta\to0$, but remain $O(1)$ for $\nu=1/2$. However, the transition between (5.22) and (5.29) as $\nu\to1/2$ is a smooth continuous one (see (5.30)), and consequently, we should not expect any discontinuity in the stability spectra between $\nu=1/2$ and $\nu\to1/2$. This has been verified through a series of calculations that are not shown here.

As noted above, although $\gamma=3$ is a good choice for most liquid and solid explosives under the equation of state assumption (2.2), it is nevertheless of interest to examine the variation in the ZND neutral stability boundaries that occur in response to a change in γ. For a CJ detonation, the effect of increasing γ is to decrease the shock pressure, consequently reducing the magnitude of the reaction rate at the shock.

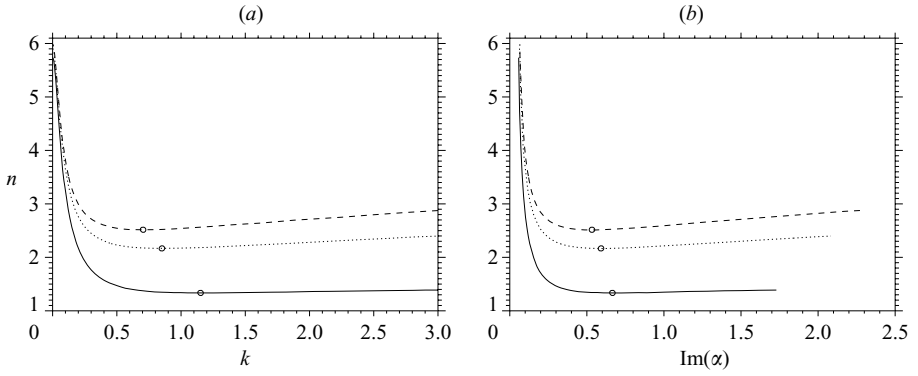

FIGURE 7. (*a*) Neutral stability boundaries in the $n - k$ plane for $k < 3$ with $f = 1$ & $\nu = 1/2$ when $\gamma = 2$ (solid), $\gamma = 3$ (dotted) and $\gamma = 4$ (dashed). The circles mark the point of two-dimensional neutral stability in the (n, k) plane. (*b*) Corresponding frequency variation along the neutral stability boundaries over the extent shown in (*a*).

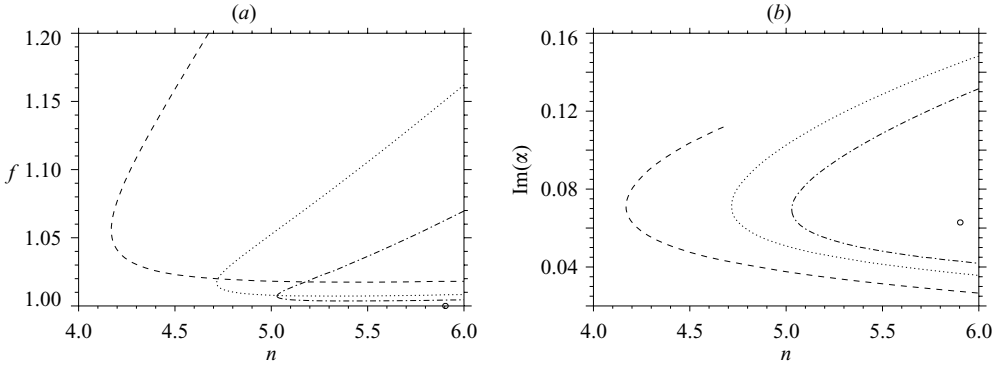

FIGURE 8. (*a*) Neutral stability boundaries in the $n - f$ plane for one-dimensional modes of different frequency identified for $\nu = 1/2$. Modes 1 (dashed), 2 (dotted) and 3 (dash-dot) are shown. The circle indicates the single point of neutral stability present for $f = 1$. The corresponding frequency variation along the extent of the neutral stability boundaries shown in (*a*) is given in (*b*).

Figure 7 shows the two-dimensional neutral stability boundaries for a CJ detonation with $\nu = 1/2$ when $\gamma = 2$, $\gamma = 3$ and $\gamma = 4$. There is a finite band of wavenumbers for which the CJ detonation is unstable for $n > 1.335$ when $\gamma = 2$, $n > 2.168$ when $\gamma = 3$, and $n > 2.516$ when $\gamma = 4$. Thus, within the confines of the idealized condensed-phase model, a detonation in a liquid or solid explosive is rendered more stable by increasing γ. Similar to the behaviour found for $\gamma = 3$, it can be seen that for both $\gamma = 2$ and $\gamma = 4$, small increases in n above the value for neutral stability results in a rapid increase in the range of wavenumbers that render the ZND detonation unstable.

Figure 8(*a*) shows the one-dimensional neutral stability boundaries in pressure sensitivity (n) and overdrive (f) space for three modes that are unstable for $f > 1$ and $\nu = 1/2$. The modes are labelled by the sequence in which they become unstable as n is increased for the range of f shown, i.e. for $f < 1.2$. For $f = 1.2$, the detonation becomes unstable to a single mode (mode 1) at $n = 4.675$, and this is the only mode that is unstable for $4.675 < n < 6$. The behaviour beyond $n = 6$ was not calculated. For $f = 1.05$, mode 1 becomes unstable at $n = 4.173$, a second mode (mode 2) becomes

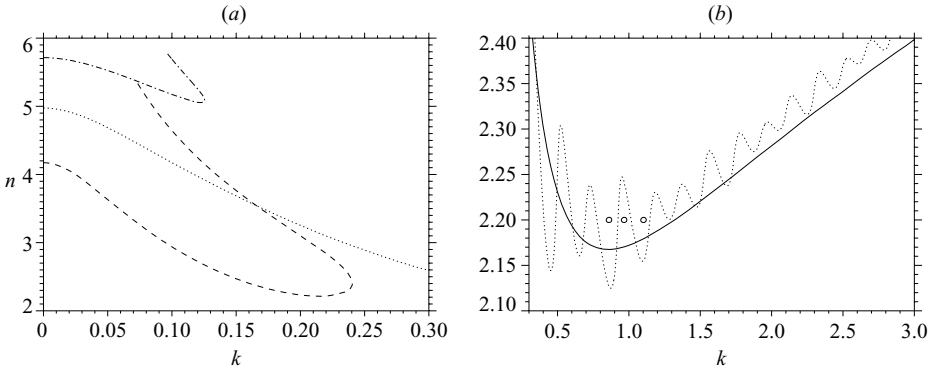

FIGURE 9. (*a*) Neutral stability boundaries in the $n-k$ plane for $f=1.05$ and $\nu=1/2$, for the first three unstable modes identified for $k=0$. (*b*) Continuation of the second mode for larger k. Also shown is the neutral stability boundary for $f=1$ and $\nu=1/2$ (solid line).

unstable at $n=4.976$, and a third mode (mode 3) becomes unstable at $n=5.714$. The corresponding frequencies of each of the modes along the neutral stability boundaries for the ranges shown in figure 8(*a*) are shown in figure 8(*b*). Of particular interest, though, is the behaviour of the neutral stability boundaries for each of the modes 1–3 as f is decreased. Concentrating first on mode 1, this mode becomes unstable for smaller values of n as f is first decreased from $f=1.2$, in common with the known stability trends of the idealized gas phase model, i.e. decreasing overdrive tends to destabilize a detonation. However, beginning with the turning point at $f=1.056$ and $n=4.170$, the mode now becomes unstable for progressively increasing values of n as f is decreased further. Even more interesting is that the boundary does not intersect the $f=1$ line, i.e. this mode is not unstable for CJ detonations, but rather reaches a minimum at $f=1.017$ when $n=5.422$. All the neutral stability boundaries associated with modes 1–3 have a similar structural behaviour. The complex behaviour that occurs close to $f=1$ associated with the bunching of multiple modes in the region $f-1\ll 1$, that is apparent in figure 8(*a*), will be detailed in a future article. In summary, for CJ detonations and $\nu=1/2$, the neutral stability point occurs when $n=5.904$, while figure 8(*a*) shows that the detonation is more unstable as the overdrive is increased away from $f=1$. In fact, for $\nu=1/2$, the ZND detonation first becomes unstable to one-dimensional disturbances for $f=1.056$ when $n=4.170$. This stability characteristic was also observed in the context of pathological detonations (Sharpe 1999). It is in contrast to the observed linear stability behaviour of ZND detonations in the idealized gas phase model, for which increasing overdrive tends to have a stabilizing effect. We also note that similar behaviour to that shown in figure 8 for $\nu=1/2$ also occurs for $\nu>1/2$.

Figure 9(*a*) shows the two-dimensional neutral stability boundaries traced out in the (n,k) plane by modes 1–3 for $\nu=1/2$ and $f=1.05$. For mode 1 and $n>2.213$, there is a finite band of wavenumbers which renders the overdriven detonation unstable. The largest wavenumber for which the detonation is unstable to mode 1 is $k=0.240$ and occurs when $n=2.397$. A similar behaviour is observed for mode 3. The behaviour for mode 2 is different. The neutral stability boundary for mode 2 for $0<k<0.3$ is shown in figure 9(*a*), and for $0.3<k<3$ in figure 9(*b*). Also shown in figure 9(*b*) is the two-dimensional neutral stability for the CJ ($f=1$) detonation. For $k>0.3$, the neutral stability boundary for mode 2 with $f=1.05$ oscillates close to that for $f=1$.

It can also be seen that for sufficiently low n there will, in general, be several distinct regions of wavenumbers where $\mathrm{Re}(\alpha) > 0$.

8. Comparison with numerical solutions: linear growth

Some comparisons between the growth rates of unstable one- and two-dimensionally perturbed ZND detonations calculated by the normal-mode analysis and those calculated from a direct numerical integration (DNI) of the reactive Euler system (2.1)–(2.4) for early times are shown below. The simulations were conducted using a new, high-order, shock-attached solution methodology described by Henrick *et al.* (2006) for one-dimensional evolutions and by Henrick (2007) for two-dimensional systems. For one-dimensional systems, the technique uses a shock-fitting strategy involving a shock-attached coordinate system. In this approach, equations (2.1)–(2.4) are solved with a method of lines formulation, employing a fifth-order Runge–Kutta temporal integration with a fifth-order mapped weighted essentially non-oscillatory (WENO) spatial scheme. Except at the shock grid point, the scheme is fully conservative. The motion of the shock is determined from an equation for the shock acceleration, given as a function of the momentum flux gradient at the shock. All other variables at the shock are then calculated in turn as functions of the shock speed through the standard shock jump conditions. At the shock, and the adjacent 2 points, special biased stencils are used to calculate flux gradients. The shock-attached strategy for two-dimensional systems is described by Henrick (2007). The shock-attached solution methodology offers some favourable advantages over standard shock-capturing algorithms for accurately capturing the evolution of unstable detonations, especially for the idealized condensed-phase model. In particular, it avoids shock 'clipping', which can dramatically affect the reaction rate W at the shock. In certain cases, the shock-capturing strategies can lead to inaccurate predictions of stability boundaries for the idealized condensed-phase model. A demonstration of this numerical issue will be presented in a future article.

All the calculations shown below were performed on a uniform spatial grid, and the resolution in each case is indicated by the number of points (pts) per half-reaction length (hrl) that are placed in the initial ZND wave. The initial conditions for the DNI solutions consisted of the ZND detonation structure for a supported CJ or overdriven detonation structure. A small-amplitude quadratic perturbation in the reaction progress variable λ is added to the ZND structure, and the system allowed to evolve in time.

8.1. *One-dimensional evolution*

Figure 10 shows the early-time evolution of the detonation shock speed D_n calculated by DNI for $f = 1$, $\nu = 1/2$ and for $n = 5.95$ and $n = 6$. Each shows a form of oscillatory, exponential growth. The growth rates and frequencies of the evolution are extracted by fitting a function of the form $D_n = a_0 + a_1 \exp(a_2 t) \sin(a_3 t + a_4)$ to the data shown in figure 10. The results of this fitting are shown in table 1 for the two cases in figure 10 as well as for $n = 5.906$. Also shown in table 1 are the corresponding predictions of the normal-mode analysis. In all cases, the agreement is excellent. Similarly good agreement is obtained for moderately overdriven waves. Cases for $\nu = 1/2$, $f = 1.1$, $n = 4.28$ and $f = 1.05$, $n = 4.5$ are shown in table 1.

8.2. *Two-dimensional evolution*

Table 2 shows a comparison between the growth rate of a two-dimensional unstable detonation for $f = 1$, $\nu = 1/2$ and $n = 2.4$, characterized by a wavelength $L = 6$

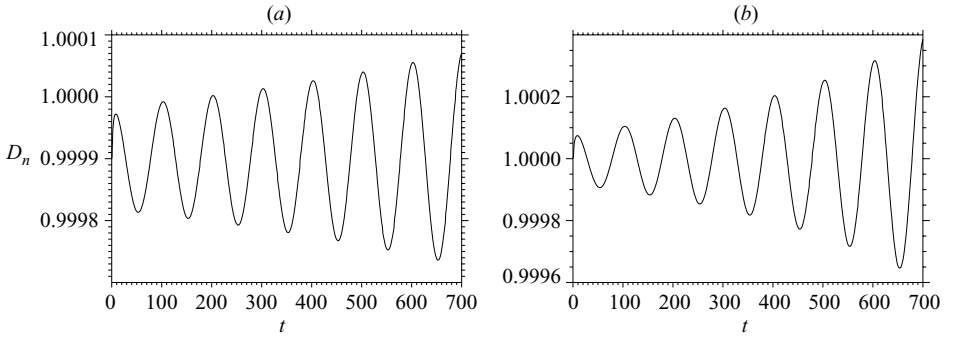

FIGURE 10. Evolution of the detonation front speed D_n for early time calculated by DNI for $f = 1$, $\nu = 1/2$, and (*a*) $n = 5.95$ and (*b*) $n = 6$. The grid resolution was 80 pts/hrl.

		Normal-mode analysis		DNI		
f	n	Re(α)	Im(α)	growth rate	frequency	res.
1	5.906	0.0000503	0.062878	0.0000502	0.062877	80
1	5.95	0.0010547	0.062870	0.0010546	0.062867	80
1	6	0.0022082	0.062837	0.0022082	0.062834	80
1.1	4.28	0.0001348	0.087987	0.0001352	0.087981	40
1.05	4.5	0.0024044	0.063625	0.0024013	0.063624	40

TABLE 1. A comparison of the growth rates and frequencies of the unstable modes predicted by the linear analysis and those calculated by high-resolution DNI. The resolution (points per half-reaction length) used in the DNI is also shown.

			Normal-mode analysis		DNI		
f	n	L	Re(α)	Im(α)	growth rate	frequency	res.
1	2.4	6	0.00908726	0.731900	0.00908759	0.731917	80
1.05	2.4	6	0.00869689	0.730839	0.00882749	0.731175	10
					0.00857121	0.730811	20
1.05	2.2	5.7	0.00152091	0.764230	0.00024641	0.763367	10
					0.00076171	0.763886	20
					0.00125331	0.764115	40
1.05	2.2	7.3	0.00244835	0.598937	0.00147256	0.598540	10
					0.00210797	0.598732	20

TABLE 2. A comparison of the growth rates and frequencies of the unstable modes predicted by the two-dimensional linear analysis and those calculated by high-resolution DNI for $\nu = 1/2$ along $z = 0$ for a periodic channel $0 \leqslant z \leqslant L$. The resolution (points per half-reaction length) used in the DNI is also shown.

(wavenumber $k = 2\pi/L = 1.0472$) as calculated via the normal-mode analysis and through a DNI using the shock-attached strategy outlined by Henrick (2007). The normal-mode growth rate variation with wavenumber for this case is given in figure 6. The direct numerical integration of the system (2.1)–(2.4) is carried in a channel of width $0 \leqslant z \leqslant L$ with periodic boundary conditions applied along $z = 0$ and $z = L$. The time evolution of the detonation shock velocity (D_n) along the boundary $z = 0$ is

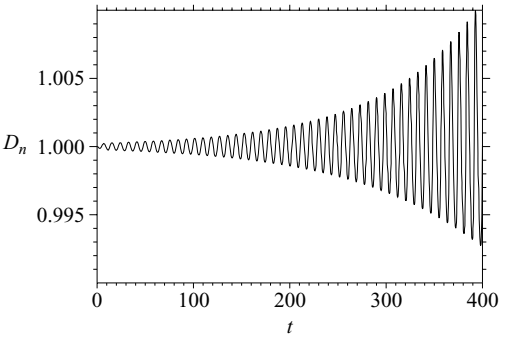

FIGURE 11. Evolution of the detonation front speed D_n for early time calculated by DNI along $z=0$ in a two-dimensional periodic channel for $f=1$, $\nu=1/2$, $n=2.4$ and $L=6$. The grid resolution was 80 pts/hrl.

given in figure 11. The agreement between the growth rates and frequencies extracted from figures 6 and 11 and shown in table 2 is again excellent.

In addition, table 2 shows comparisons between a DNI of (2.1)–(2.4) and the normal-mode solutions for three overdriven cases in a two-dimensional periodic channel ($0 \leqslant z \leqslant L$). It should be noted that the resolution used in the overdriven cases is lower than that typically employed for the Chapman–Jouguet simulations. The overdriven detonation wave simulations are conducted on significantly larger domains to prevent any numerically spurious reflections of disturbances from the downstream outflow boundary over a given time span, which we have shown can affect the linear evolution of the wave. For the case with $f=1.05$, $n=2.4$ and $L=6$, the agreement between the growth rates and frequencies is excellent given the 20 pts/hrl resolution. The two cases with $f=1.05$, $n=2.2$ and either $L=5.7$ or $L=7.3$ lie close to the two-dimensional neutral stability boundary (figure 9*b*). The agreement between the frequencies is excellent. It is also satisfactory for the growth rates, which are clearly converging towards the normal-mode results under increasing resolution. In particular, the two cases for $f=1.05$ and $n=2.2$ with channel widths of $L=5.7$ and $L=7.3$ lie within two neighbouring unstable regions of the oscillatory variation in the neutral stability boundary location (the locations of the two cases are marked by the circles in figure 9*b*). Moreover, a DNI for $f=1.05$, $n=2.2$ and $L=6.5$ (also marked by a circle in figure 9*b*) reveals that the detonation is linearly stable, a confirmation of the validity of the unusual wavy variation shown in figure 9(*b*) for $f=1.05$. In summary, we have demonstrated an excellent agreement between the growth rates and frequencies of unstable disturbances obtained from a normal-mode analysis and from a direct numerical integration for both Chapman–Jouguet and overdriven systems with square-root depletion ($\nu=1/2$). Other cases we have calculated for $\nu>1/2$ show similarly excellent agreement.

8.3. *Stable evolution for* $\nu=1/2$

It was noted in § 6.2 that stable modal solutions of the exponential form (4.5) can formally exist for the case of $\nu=1/2$ and $f=1$. Figure 12(*a*) shows the evolution of the detonation shock speed in time for $f=1$, $\nu=1/2$ and $n=5.9$ calculated from a numerical simulation of (2.1)–(2.4) using the methodology described above. For this case, $K_p=-0.002892$ (see § 6.2). A calculation from the linear stability analysis shows that $\mathrm{Re}(\alpha)=-8.60\times10^{-5}$ and $\mathrm{Im}(\alpha)=0.062878$, so that $K_p<\mathrm{Re}(\alpha)<0$. An exponential fit of the form described in § 8.1 to the slowly decaying amplitude of

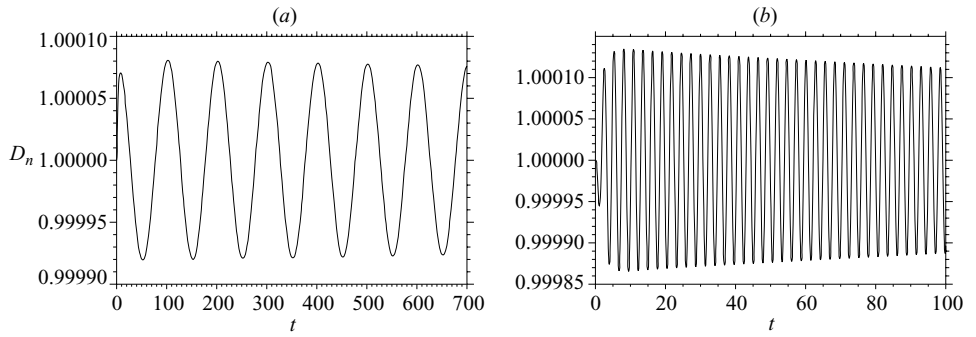

FIGURE 12. Detonation front speed D_n for early time calculated by DNI for $f=1$, $\nu=0.5$: (*a*) one-dimensional evolution for $n=5.9$; (*b*) two-dimensional periodic channel evolution along $z=0$ for $n=2.4$ and $L=1.9$. The grid resolution was 80 pts/hrl in each case.

D_n in figure 12(*a*) gives $\mathrm{Re}(\alpha)=-8.61\times10^{-5}$ and $\mathrm{Im}(\alpha)=0.062877$, an excellent agreement between the two results. Figure 12(*b*) shows the decay in amplitude of D_n along $z=0$ arising after a weak perturbation of the steady ZND wave for $f=1$, $n=2.4$ and $\nu=1/2$ in a periodic two-dimensional channel with $L=1.9$. For this case, $K_p=-0.024134$. For a periodic channel of width $L=1.9$, the wavenumber $k=3.3069$. A linear stability analysis calculation gives $\mathrm{Re}(\alpha)=-0.0019355$ and $\mathrm{Im}(\alpha)=2.295462$ for these parameters. A fit to the numerical solution shown in figure 12(*b*) gives $\mathrm{Re}(\alpha)=-0.0019365$ and $\mathrm{Im}(\alpha)=2.295464$. These results show that for $f=1$ and $\nu=1/2$, modal solutions of the exponential form (4.5) are possible provided $K_p<\mathrm{Re}(\alpha)<0$ and that the agreement between the linear stability analysis and a numerical simulation of the early-time damping behaviour of D_n is excellent.

9. Nonlinear evolution of unstable Chapman–Jouguet detonations for the idealized condensed-phase model

In the final section, we discuss some long-time evolution calculations of one-dimensional pulsating and two-dimensional unstable Chapman–Jouguet detonations for the idealized condensed phase model. Again, these are calculated by direct numerical integration of equations (2.1)–(2.4) using the shock-fitting, shock-attached strategy (Henrick *et al.* 2006; Henrick 2007).

9.1. *Pulsating instabilities*

Figures 13, 14 and 15 show the long-time evolution of the detonation shock speed of an initially supported, steady CJ detonation for $\nu=1/2$, and $n=5.95$, $n=5.975$ and $n=6$. For $n=5.95$ (figure 10), the linear stage of the growth persists over a long time, due to the slow growth rate of the unstable mode ($\mathrm{Re}(\alpha)=0.00105$). The growth initially appears to saturate at around $t=4500$, but there is a second growth stage for $5500<t<6500$, before the oscillatory amplitude of D_n saturates, and the detonation front enters a periodic limit cycle state with period $T=91.8$ and an amplitude of around 3.5% of the initial CJ velocity. The late-time periodic behaviour for $(39000<t<40000)$ is shown in the $(\mathrm{d}D_n/\mathrm{d}t, D_n)$ phase portrait in figure 16(*a*). The evolution of D_n for $n=5.975$ is shown in figure 14. The initial stages of the nonlinear saturation behaviour appear to indicate a 'beating' form of evolution, but the amplitude of the beating cycle decays in time and for $t>40000$, the shock speed evolution appears to have limited to a single-mode periodic state. The phase portrait

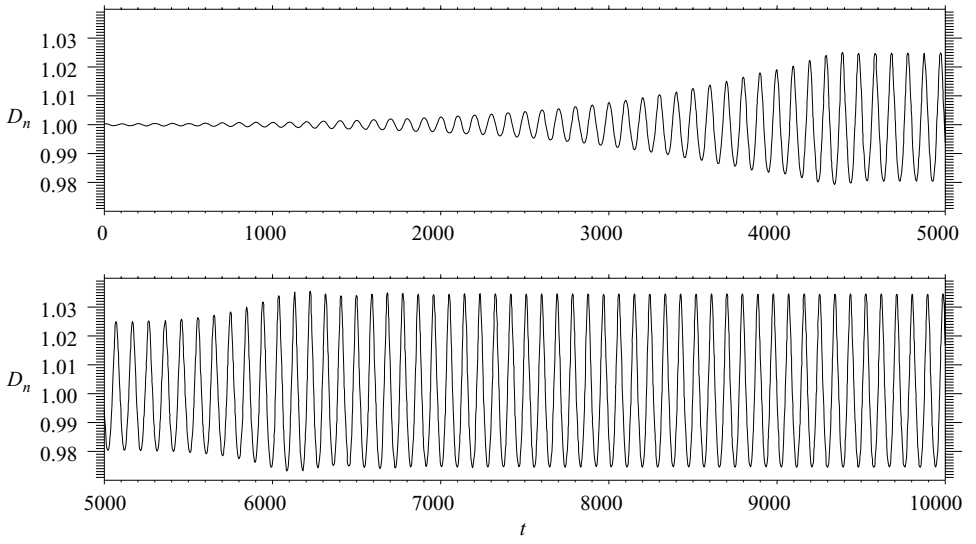

FIGURE 13. Long-time evolution of the detonation front speed calculated by DNI for $f = 1$, $\nu = 1/2$ and $n = 5.95$. The grid resolution was 40 pts/hrl.

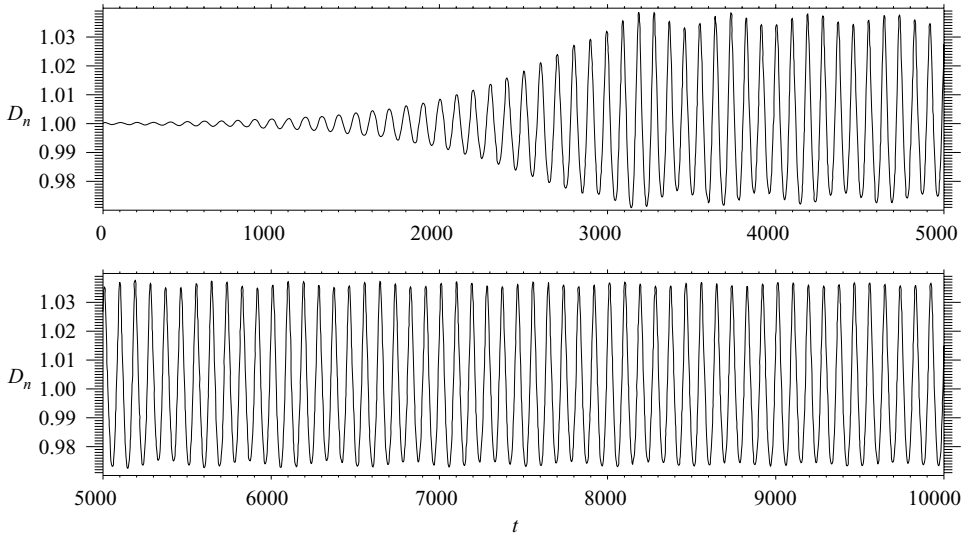

FIGURE 14. Long-time evolution of the detonation front speed calculated by DNI for $f = 1$, $\nu = 1/2$ and $n = 5.975$. The grid resolution was 40 pts/hrl.

for $n = 5.975$ where $39000 < t < 40000$ is shown in figure 16b. The evolution of D_n for $n = 6$ is shown in figure 14. After the nonlinear saturation point for $t > 2500$, there is a sustained 'beating' form of evolution in the amplitude variation of D_n. The total amplitude variations of the oscillation in D_n are approximately 4% of the initial CJ speed, with the beating oscillation having an amplitude of about 1% of the initial CJ speed. In this case, we do not observe any decay of the beating cycle, and there is no evidence of any periodic behaviour for $t < 60000$. This apparently multi-mode evolution is observed in the phase portrait shown in figure 16(c) for $39000 < t < 40000$. A striking feature of the above nonlinear one-dimensional dynamics (which is repeated

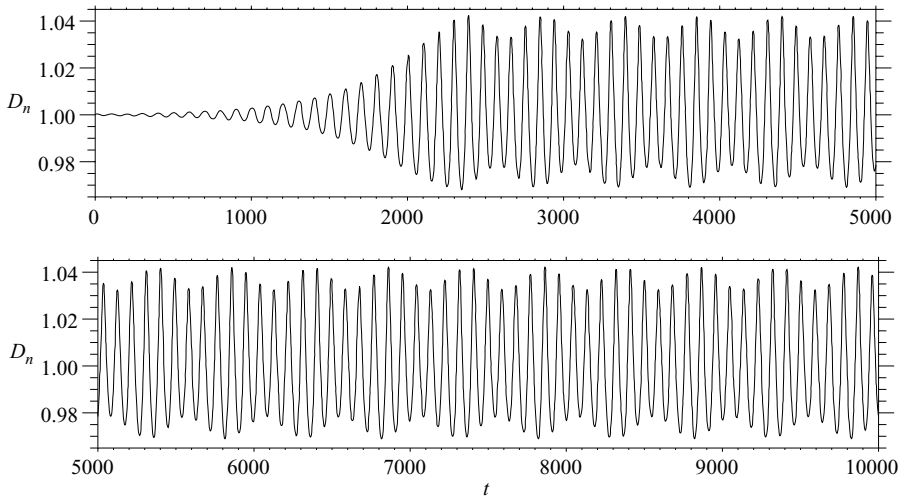

FIGURE 15. Long-time evolution of the detonation front speed calculated by DNI for $f = 1$, $\nu = 1/2$ and $n = 6$. The grid resolution was 40 pts/hrl.

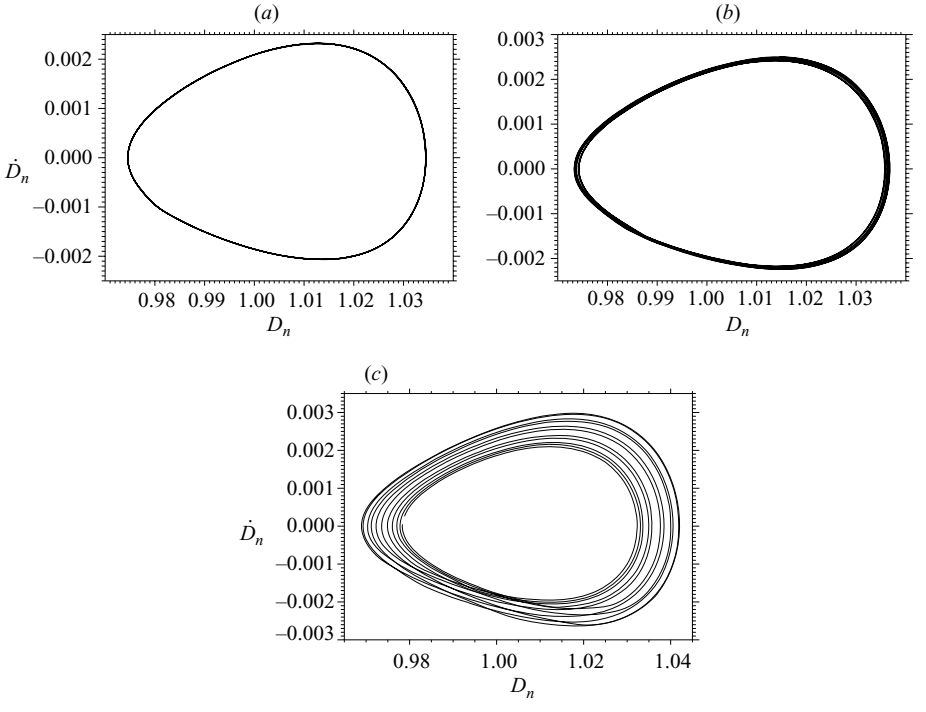

FIGURE 16. Phase plane $(\mathrm{d}D_n/\mathrm{d}t, D_n)$ representation of the detonation front evolution calculated by DNI for $f = 1$, $\nu = 1/2$ and (*a*) $n = 5.95$, (*b*) $n = 5.975$ and (*c*) $n = 6$. The time interval over which each phase plane is shown is $t \in [39000, 40000]$. The grid resolution was 40 pts/hrl.

for a range of other simulations we have conducted) is the relatively small magnitude of the detonation shock velocity departures in the saturated nonlinear equilibrium state from the underlying ZND value ($D_n = 1$) as the pressure exponent (n) is increased

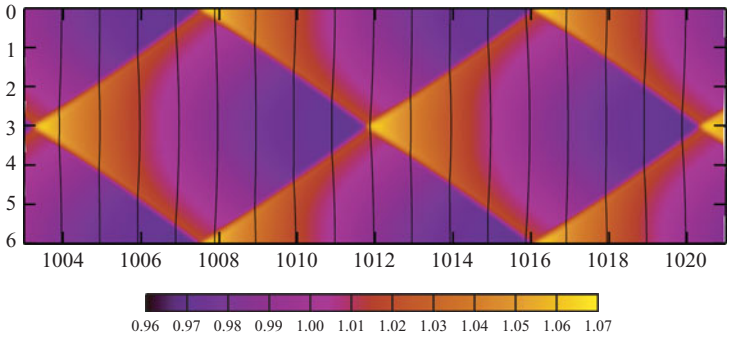

FIGURE 17. Evolution of the detonation front speed D_n in time for $f=1$, $\nu=0.5$ and $n=2.4$ in a periodic channel $0\leqslant z\leqslant L$, where $L=6$. The black lines are the locus of the incident shock.

significantly from its neutrally stable value. This property is markedly different to that previously observed for one-dimensional pulsating detonations in the idealized gas phase model.

9.2. *Cellular instabilities*

Figure 17 shows the long-time evolution of the detonation shock speed (D_n) corresponding to the case shown in figure 11, i.e. for a two-dimensional unstable detonation with $f=1$, $n=2.4$ and $\nu=1/2$ in a channel $0\leqslant z\leqslant 6$, with periodic boundaries on $z=0$ and $z=6$. A cellular, diamond-like, pattern is clearly evident in the channel that is reminiscent of the dynamics of cellular detonations formed under the idealized gas phase model. Along any line of fixed z, the evolution involves alternating periods of shock acceleration and deceleration. The black lines in figure 17 show the locus of the incident shock at various times in the evolution. There are several interesting features to this plot; the first is the relatively small deflections in the shock locus across the channel. The second is the relatively small departures of the detonation shock velocity from the steady CJ value $D_n=1$ (up to 7%). Finally, the time scale over which a complete detonation cell is formed is 8.6, as determined from figure 17. This compares to the linear analysis where the completion of a period in the detonation speed along any fixed z, occurs over a time scale of $2\pi/\mathrm{Im}(\alpha)=2\pi/0.7319=0.858$ (table 2), almost identical to that recovered from the simulation. Further insights into the reason for the small deflections in the shock locus across the channel can be obtained from figure 18, which shows various snapshots of the density variation behind the incident shock during the cell cycle. Transverse shock waves and slip lines are clearly evident in a triple-point configuration; however, the gradient discontinuity in the incident shock locus is small at the shock intersection point. Figure 19 shows snapshots of density and pressure variations at one time superimposed with constant pressure and density contours, demonstrating that the transverse shock wave is weak in amplitude.

10. Summary

A linear stability analysis of CJ and moderately overdriven detonations ($f>1$, $f-1=O(1)$) of ZND type has been conducted within the context of a general model that incorporates the idealized gas phase and condensed-phase models. The idealized

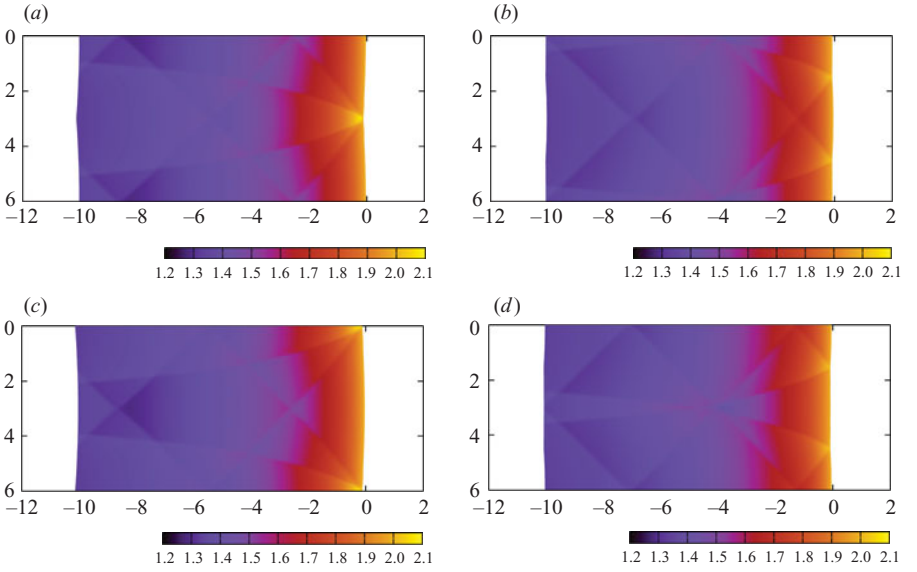

FIGURE 18. Snapshots of the density variation behind the detonation front in the periodic channel $0 \leqslant z \leqslant 6$. The variations are shown in the longitudinal coordinate frame $x = x^l - Dt$. The snapshots are taken at the times (*a*) $t = 1003.40$, (*b*) $t = 1005.55$, (*c*) $t = 1007.71$ and (*d*) $t = 1009.86$.

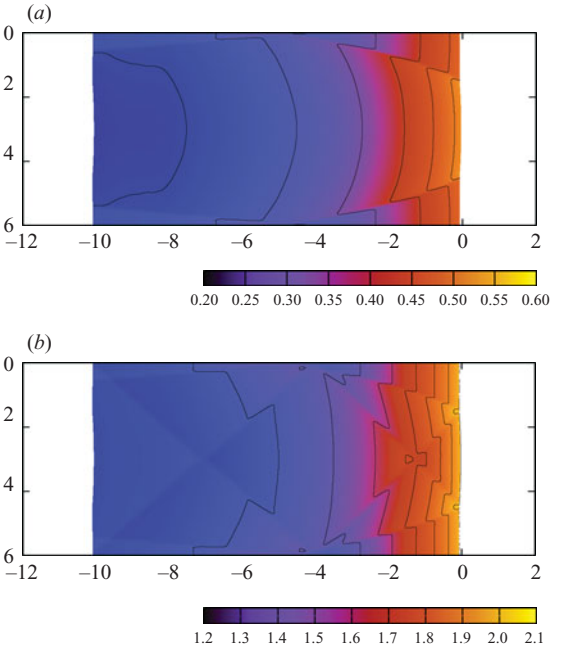

FIGURE 19. Snapshots of pressure (*a*) and density (*b*) variations at $t = 1005.55$. The black lines indicate contours of constant pressure (with values, from left to right, of 0.25 to 0.50 in steps of 0.05) and density (with values, from left to right, of 1.4 to 2.0 in steps of 0.1).

condensed-phase model is a basic model that is often used for the purposes of mathematical analysis of detonation wave dynamics in condensed-phase systems. We have provided a detailed examination of the spatial boundedness closure conditions that are required for the linear stability analysis of the general model. These govern the behaviour of the perturbation quantities at the end of the reaction zone for reaction orders ν in the range $1/2 \leqslant \nu \leqslant 1$. The results of the linear analysis highlight several differences in the global properties of the stability spectra between idealized condensed and gas phase detonations. These include: the presence of only a single unstable mode for CJ waves, and overdriven ZND waves that are more unstable than the CJ waves. The results of the normal-mode analysis and those obtained from early-time direct numerical integrations of unstable detonations defined by the idealized condensed-phase model agree well. The case of weakly overdriven systems where $f > 1$, $f - 1 \ll 1$, for which further difficulties arise in constructing the spatial boundedness conditions for the linear analysis, will be considered in a future article.

For the idealized condensed-phase model, long-time direct numerical integrations reveal that for unstable, one-dimensional CJ detonations, the evolution occurs in a form of pulsating instability, while for unstable two-dimensional detonations, detonation cells appear to form. However, although these dynamics are apparently similar to those observed for unstable detonations in the idealized gas phase model, in both the one- and two-dimensional cases for the idealized condensed-phase model, the amplitude of the shock velocity deviations from its ZND value are relatively small (typically of the order of a few per cent) even in the saturated long-time solution. Also, in the two-dimensional case, the deflection in the shock locus angle at a point of triple shock interaction is weak. These represent significant deviations from the nonlinear dynamics of unstable detonations for the idealized gas phase model. Finally, from a practical viewpoint, when the idealized condensed-phase model is used to mimic real explosive systems, such as liquid nitromethane or solid PBX-9501, where a choice of $\nu = 1/2$ and a pressure sensitivity in the range $n = 1 - 3$ is normally employed (Bdzil *et al.* 2003), a planar CJ detonation would only be stable to multi-dimensional disturbances when the pressure sensitivity $n < 2.168$.

MS and IIA were supported by DOE LANL and AFOSR, while TDA, JBB and GJS were supported by DOE LANL. GJS also received funding from EPSRC and DSTL.

REFERENCES

Bdzil, J. B., Aslam, T. D., Henninger, R. & Quirk, J. J. 2003 High-explosive performance: Understanding the effects of finite-length reaction zone. *Los Alamos Science* **28**, 96–110.

Bdzil, J. B., Short, M., Sharpe, G. J., Aslam, T. D. & Quirk, J. J. 2006 Higher-order DSD for detonation propagation: DSD for detonation driven by multi-step chemistry models with disparate rates. In *Proc. Thirteenth Symposium (Intl) on Detonation*. Office of Naval Research Rep. ONR 351-07-01, pp. 726–736.

Bourlioux, A. & Majda, A. J. 1992 Theoretical and numerical structure for unstable two-dimensional detonations. *Combust. Flame* **90**, 211–229.

Bourlioux, A., Majda, A. J. & Roytburd, V. 1991*a* Theoretical and numerical structure for unstable one-dimensional detonations. *SIAM J. Appl. Maths* **51**, 303–343.

Bourlioux, A., Majda, A. J. & Roytburd, V. 1991*b* Nonlinear development of low frequency one-dimensional instabilities for reacting shock waves. In *Dynamical Issues in Combustion Theory* (ed. P. C. Fife, A. Linan & F. A. Williams). IMA Volumes in Mathematics and its Applications, vol. 35, pp. 63–82.

Clavin, P. & He, L. T. 1996 Stability and nonlinear dynamics of one-dimensional overdriven detonations in gases. *J. Fluid Mech.* **306**, 353–378.

Clavin, P., He, L. T., & Williams, F. A. 1997 Multidimensional stability analysis of overdriven gaseous detonations. *Phys. Fluids* **9**, 3764–3785.

Clavin, P. & Williams, F. A. 2002 Dynamics of planar gaseous detonations near Chapman–Jouguet conditions for small heat release. *Combust. Theory Model.* **6**, 127–139.

Daou, R. & Clavin P. 2003 Instability threshold of gaseous detonations. *J. Fluid Mech.* **482**, 181–206.

Davis, W. C. 1981 Fine structure in nitromethane/acetone detonations. In *Proc. Seventh Symposium (Intl) on Detonation*, pp. 958–964.

D'yakov, S. 1954 The stability of shock waves: Investigation of the problem of the stability of shock waves in arbitrary media. *Zh. Eksp. Teor. Fiz.* **27**, 288.

Engelke, R. & Bdzil, J. B. 1983 A study of the steady-state reaction-zone structure of a homogeneous and a heterogeneous explosive. *Phys. Fluids* **26**, 1210–1221.

Erpenbeck, J. J. 1964 Stability of idealized one-reaction detonations. *Phys. Fluids* **7**, 684–696.

Fickett, W. & Davis, W. C. 1979 *Detonation.* University of California Press.

Gamezo, V. N., Vasil'ev, A. A., Khokhlov, A. M. & Oran, E. S. 2000 Fine cellular structures produced by marginal detonations. *Proc. Combust. Inst.* **28**, 611–617.

Gorchkov, V., Kiyanda, C. B., Short, M. & Quirk, J. J. 2007 A detonation stability formulation for arbitrary equations of state and multi-step reaction mechanisms. *Proc. Combust. Inst.* **31**, 2397–2405.

Gustavsen, R. L., Sheffield, S. A., & Alcon, R. R. 2000 Progress in measuring detonation wave profiles in PBX-9501. In *Proc. Eleventh Symposium (Intl) on Detonation.* Office of Naval Research Rep. ONR 3330000-5, pp. 821–827.

Henrick, A. K. 2007 Shock-fitted solutions for two-dimensional detonation. PhD Thesis, University of Notre Dame.

Henrick, A. K., Aslam, T. D. & Powers, J. M. 2006 Simulations of pulsating one-dimensional detonations with true fifth order accuracy. *J. Comput. Phys.* **213**, 311–329.

Hill, L. G., Bdzil, J. B & Aslam, T. D. 2002 Front curvature rate stick measurements and detonation shock dynamics calibration for PBX-9502 over a wide temperature range. In *Proc. Eleventh Symposium (Intl) on Detonation.* Office of Naval Research Rep. ONR 33300-5, pp. 1029–1037.

Klein, R. 1991. On the dynamics of weakly curved detonations. In *Dynamical Issues in Combustion Theory* (ed. P. C. Fife, A. Linan & F. A. Williams). IMA Volumes in Mathematics and its Applications, vol. 35, pp. 127–166.

Kontorovich, V. 1957 Concerning the stability of shock waves. *Zh. Eksp. Teor. Fiz.* **33**, 1525.

Lee, E. L. & Tarver, C. M. 1980 Phenomenological model of shock initiation in heterogeneous explosives. *Phys. Fluids* **23**, 2362–2372.

Lee, H. I. & Stewart, D. S. 1990 Calculation of linear instability: One-dimensional instability of plane detonation. *J. Fluid Mech.* **216**, 103–132.

Majda, A. & Roytburd, V. 1992 Low-frequency multidimensional instabilities for reacting shock-waves. *Stud. Appl. Maths* **87**, 135–174.

Ng, H. D., Higgins, A. J., Kiyanda, C. B., Radulescu, M. I., Lee, J. H. S., Bates, K. R. & Nikiforakis, N. 2005 Nonlinear dynamics and chaos analysis of one-dimensional pulsating detonation. *Combust. Theory Model.* **9**, 159–170.

Radulescu, M. I., Ng, H. D., Lee, J. H. S. & Varatharajan, B. 2002 Effect of argon dilution on the stability of acetylene-oxygen detonations. *Proc. Combust. Inst.* **29**, 2825–2831.

Roberts, A. E. 1945 Stability of a plane steady shock. Los Alamos National Rep. 299. Los Alamos National Laboratory.

Roe, P. 1998 Linear bicharacteristic schemes without dissipation. *SIAM J. Sci. Comput.* **19**, 1405–1427.

Sanchez, A. L., Carretero, M., Clavin, P. & Williams, F. A. 2001 One-dimensional overdriven detonations with branched-chain kinetics. *Phys. Fluids* **13**, 776–792.

Seitz, W. L., Stacy, H. L., Engelke, R., Tang, P. K. & Wackerle, J. 1989 Detonation reaction zone structure of PBX9502. In *Proc. Ninth Symposium (Intl) on Detonation.* Office of Naval Research Rep. ONR 113291-7, pp. 657–669.

Sharpe, G. J. 1997 Linear stability of idealized detonations. *Proc. R. Soc. Lond.* A **453**, 2603–2625.

Sharpe, G. J. 1999 Linear stability of pathological detonations. *J. Fluid Mech.* **401**, 311–338.

Sharpe, G. J. 2001 Transverse waves in numerical simulations of cellular detonations. *J. Fluid Mech.* **447**, 31–51.

Sharpe, G. J. & Falle, S. A. E. G. 1999 One-dimensional numerical simulations of idealized detonations. *Proc. R. Soc. Lond.* A **455**, 1203–1214.

Sheffield, S. A., Engelke, R., Alcon, R. R., Gustavsen, R. L., Robbins, D. L., Stahl, D. B., Stacy, H. L. & Whitehead, M. C. 2002 Particle velocity measurements of the reaction zone in nitromethane. In *Proc. Twelfth Symposium (Intl) on Detonation.* Office of Naval Research Rep. ONR 333-05-02, pp. 159–166.

Short, M. & Blythe, P. A. 2002 Structure and stability of weak-heat-release detonations for finite Mach numbers. *Proc. R. Soc. Lond.* A **458**, 1795–1807.

Short, M. & Dold, J. W. 1996 Multi-dimensional linear stability of a detonation wave with a model three-step chain-branching reaction. *Math. Comput. Model.* **24**, 115–123.

Short, M. & Quirk, J. J. 1997 On the nonlinear stability and detonability limit of a detonation wave for a model 3-step chain-branching reaction. *J. Fluid. Mech.* **339**, 89–119.

Short, M. & Sharpe G. J. 2003 Pulsating instability of detonations with a two-step chain-branching reaction model: Theory and numerics. *Combust. Theory Model.* **7**, 401–416.

Short, M. & Stewart, D. S. 1998 Cellular detonation stability. Part 1. A normal-mode linear analysis. *J. Fluid Mech.* **368**, 229–262.

Short, M. & Stewart, D. S. 1999 The multi-dimensional stability of weak-heat-release detonations. *J. Fluid Mech.* **382**, 109–135.

Tarver, C. M., Kury, J. W. & Breithaupf, R. D. 1997 Detonation waves in triaminotrinitrobenzene. *J. Appl. Phys.* **82**, 3771–3782.

Wasow, W. 2002 *Asymptotic Expansions for Ordinary Differential Equations.* Dover.

Yao, J. & Stewart, D. S. 1996 On the dynamics of multi-dimensional detonation. *J. Fluid Mech.* **309**, 225–275.